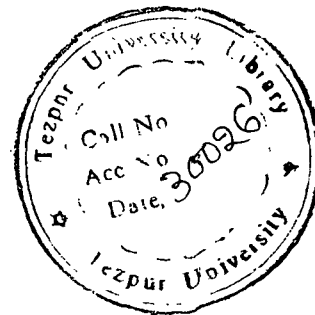# DESIGN OF AN IMPROVED SCANNING OPTICAL MICROSCOPE (SOM)
AND
ADAPTATION OF SECOND HARMONIC GENERATION

BY
ANJALI SARMAH (GOSWAMI), M. Sc
Registration No. 118 of 2004(T.U)

Submitted in partial fulfillment of the requirements
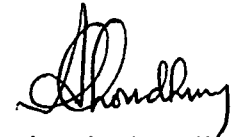for
The Degree of Doctor of Philosophy
September, 2006

In
School of Science & Technology
Department of Physics
Tezpur University
Napaam, Tezpur

535.84
SAR

CERTIFICATE

This is to certify that the thesis entitled "Design of an improved Scanning Optical Microscope (SOM) and adaptation of second harmonic generation" being submitted by Anjali Sarmah (Goswami) to Tezpur University, Napaam, Tezpur, Assam in fulfillment of the requirements for the award of the degree of Doctor of Philosophy, is a record of original bonafide research work carried out by her. She has worked under my guidance and supervision and has fulfilled the requirements for the submission of this thesis. The results contained in the thesis have not been submitted in part or full to any other university or institute for award of any degree or diploma.

20.9.06

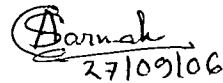(Amarjyoti Choudhury)

Professor,

Department of Physics,

Tezpur University,

Tezpur- 784028 (Assam)

DECLARATION

I hereby declare that the thesis entitled "Design of an improved Scanning Optical Microscope (SOM) and adaptation of second harmonic generation" being submitted to the Department of Physics, Tezpur University, Tezpur, Assam in partial fulfillment of the requirements for the Degree of Philosophy, has previously not formed the basis for the award of any degree, diploma, fellowship or any other similar title or recognition.

September, 2006

Anjali Sarmah (Goswami)

Department of Physics,

Tezpur University,

Tezpur- 784028 (Assam)

PREFACE

This thesis presents the design consideration of an improved scanning optical microscope (SOM) and its adaptation to the second harmonic mode of imaging. The basic principle of the modern scanning optical microscope is that the intense beam of laser light is focused to a diffraction-limited spot and is used to scan the specimen, point by point in a raster form. The transmitted or the reflected light is detected by a photo-detector, which converts the optical signal to the electric signal. These signals are processed and then displayed on a monitor as image.

Very high power density of the scanning spot of the SOM due to the use of focused laser light gives rise to second harmonic generation from non-linear specimen having no centro- symmetricity. Detecting these signals and then constructing images of different samples, second harmonic mode of imaging can be adapted on the SOM. Our work mainly consists of designing the scanning optical microscope of improved type with reference to mode of scanning and its adaptation for second harmonic imaging. To improve the resolution we make the confocal arrangement also.

In **chapter I**, we introduce these ideas having relevance to the work of scanning optical microscope and also furnish the stages of its gradual improvement.

Chapter II contains the complete designing technique of the scanning optical microscope. In this chapter, we also discuss how the microscope can be improved for confocal imaging, 3-d imaging through z-movement of the objective and also how the second harmonic imaging mode can be adapted.

Chapter III is the review of the theoretical part of the scanning optical microscope and second harmonic generation.

In **chapter IV**, we devote ourselves to experimental work as regards the comparison of the images of designed conventional SOM with those of the second harmonic scanning optical microscope (SHSOM) and also those of the confocal SOM and some applications of SHSOM.

Chapter V includes a look into the future as regards improved design and application of second harmonic microscope in studying material as well as biological samples.

Anjali Sarmah (Goswami)

22nd September, 2006

Tezpur

Acknowledgement

Contents

CHAPTER III

THEORETICAL REVIEW

CHAPTER IV

COMPARISONAL STUDY OF THE IMAGES OF CONVENTIONAL SOM WITH THOSE OF SHSOM AND CONFOCAL SOM AND SOME APPLICATIONS OF SHSOM

LIST OF FIGURES

CHAPTER II:

Results as follows:

Using low power source

Using low power He-Ne source

Using high power Nd- Yag source; detector :PMT

Using high power Nd- Yag source; detector: Silicon photodiode UDT Model PIN-100

CHAPTER I

INTRODUCTION

1.1. Introduction:

The long and exciting history of development of the microscope indicates that the earliest design in its simple form can be attributed to Roger Bacon and his contemporary Salvino Degli Armati[1] in the 13th century, though there are claims that the microscope is a gift of the Chinese civilization. Three spectacle makers Hans Jausen, his son Zacharias and Hans Lippershey[2] of Netherlands have received the credit for the invention of compound microscope some time between 1590 and 1608. Since then its improvement is continuing till now which is the era of far-field scanning optical microscope, near field scanning optical microscope, scanning electron microscope, scanning tunneling microscope, atomic force microscope etc and thus it becomes a very powerful tool in scientific development

The scanning optical microscope(SOM) is a device in which a diffraction limited on-axis spot of laser beam scans the specimen; the transmitted or the reflected beam from the specimen is detected by a photo detector. The voltage-time signals detected by the photo detector are converted to the point by point image of the specimen as processed through some electronic devices and monitored on CRO screen or computer.

The advantage of using a scanning approach in optical microscope can be listed in brief as follows:

1

1. Possibility of enhanced imaging through modification of the optical system.

2. Better lateral resolution.

3. Better contrast. Staining is not required in the biological sample for contrast.

4. Use of wide range of wavelength.

5. Possibility of studying non-linear properties of material through second harmonic imaging.

6. Achievement of super-resolution.

7. Optical sectioning property through confocal imaging which results in three dimensional imaging property.

8. Optical Beam Induced Current(OBIC) facilities, delineation of p-n junctions.

9. Possibility of transmission over a large distance, storing in magnetic-tap and the large display in a CRO or computer desktop.

10. Sequential imaging which is readily suited for image processing in computer.

1.2. Review of literature:

As we go through the history of scanning optical microscope it is found that Young and Roberts[3] first introduced the scanning concept in microscopy in 1951 by

designing a flying spot microscope. They used the demagnified (by an objective lens of a microscope) scanning spot of a cathode ray tube to scan the specimen and the transmitted light from the specimen was detected by a photocell. The resultant video signal was displayed on a CRT monitor. After Roberts and Young, contribution of many scientists leads this scanning mechanism in microscopy to the present highly improved status which is discussed briefly as follows.

R. Barer [4] and Hundley [5] added the idea of interference microscopy in scanning system in 1952. Laub [6] contributed scanning differential microscope. Polze [7] designed a laser interference microscope

In 1955 Deely [8] used mechanical scanning of an aperture and photomultiplier tubes as detector which showed the potentiality of SOM in quantitative measurement. This idea of quantitative measurement was applied by many scientists latter on such as Box and Freund [9] adopted a flying spot microscope for this purpose. Dobrowolski et al [10] used SOM for the measurement of the Diameter of the opaque cylinder. Slater [11], with the help of Airy disc measured the sub- micron circular aperture. Welford [12] used SOM for the consideration of rough measurement at the optical limit.

In biology, ultra-violet microscopy has an important role. Montogomery [13] constructed a flying spot microscope in which he used an ultra violet emitting scanner tube. It prevents the damage of biological sample due to toxicity of u-v light in conventional microscope in which photographic recording technique is such that it

requires large exposures. Some other scientists also used ultra violet microscopy through different types of technology. Zworykin [14] in 1957 constructed a u-v colour transmitting microscope by using three u-v wavelengths. He used a television camera tube as a detector. Mellors and Silver constructed a microscope with Nipkow wheel scanning arrangement for u-v fluorescence microscopy. Later on, this was reviewed by Price and Schwartz [15]. Freed used a vibratory mirror scanning system for u-v microscopy.

Minsky [16] in his reflection and transmission model of scanning microscope scanned the specimen mechanically and light from the specimen was focused through a small aperture which ensured that the information is obtained from one particular level of the specimen. To ensure that light is collected from one depth level, Egger and Petran [17] used a nipkow wheel for scanning, such that light was made to pass through the wheel before and after striking the specimen. With the help of this arrangement, one section of a thick specimen can be studied. The scanning can be achieved by the movement of the specimen or of a lens in the optical path. This idea was given by Casperson [18] and Davidovitz [19,20]constructed a microscope using the second method for scanning. They made arrangement for providing adequate signal to noise ratio. Beyer [21] discussed the application of laser microscope to biology.

4

Optical heterodyne techniques had been combined with the scanning microscopy for phase and amplitude sampling of coherent light field in 1969 by Korpel and Whitman [22].

The name of another scientist, Petran has to be cited for mentioning the possibility of super-resolution in S.O M., which was later on explored by Ash and Nicholls [23] with the help of super resolution aperture scanning microscopy at optical frequencies.

Laser scanning microscope for pyro-electric image display in real time was reported by Handi [24] and used for the study of distribution of domains in ferroelectric crystals.

A group of research workers under the supervision of R. Kompfner and C.J R. Sheppard [25] in Oxford University designed out a new variety of SOM for studying transparent object In 1977, R.Kompfner, C J.R. Sheppard and A. Choudhury [26] in Oxford University attempted to construct image in scanning optical microscope using Fourier Techniques to achieve better designing of SOM, including the reflection mode of imaging. They reported both theoretically and experimentally, the two types of scanning optical microscope. Those were Type-I and Type-II. The later is also known as confocal scanning optical microscope. Different aspects of viewing an object in its own second harmonic light were also mentioned by A. Choudhury [27].

From confocal microscopy, another important idea has been investigated by Brakenhoff [28] et al (1980). This is the idea of image slices through thick object

Carlsson [29] et al in 1985 have recorded image slices using confocal fluorescence microscopy and processed these digitally to form stereoscopic image pairs.

The optical sectioning property allows the use of three further imaging techniques:

The extended focus (Wilson and Hamilton [30], 1982; Sheppard et al, 1983 [31])

The automatic focus (Cox and Sheppard, 1983b [32]), technique which increases the depth of field with high resolution.

The third one is surface profiling technique (Caulfield and Kryger, [33] 1978; Hamilton and Wilson, 1982a [34]; Cox and Sheppard, 1983b [32]) allows investigation of surface topography.

H. Rohrer and G. Binnig [35] were awarded the Nobel prize for their invention of scanning tunneling microscope in 1981.

The discovery of the idea of near- field optical microscopy has to be credited to Synge [36]. Using this idea in the scanning mechanism, gives rise to the scanning near-field optical microscopy. Vast research works are going on in this field and the name of only few scientists are mentioned as follows:

T. Pagnot, D. Barchiesi, D.V. Labeke, C.Pieralli, et al [37].

Ulrich D. Keil, Jacob R. Jenson and Jorn M. Hvam [38] et al are working on fibre coupled ultra fast scanning tunneling microscope.

Atomic force imaging technique was invented by Binnig , Quate and Gerber [39] in which also the scanning mechanism was used.

The scanning exploration for computer image construction was supported by Ash [40]

The advent of Q-switched laser made it possible to obtain real SHG photograph of triglycine sulphate crystal [41] and Dauphine twins in quartz [42]. The structure of polycrystalline ZeSe was first observed by Hellwarth and Christiansen by using SHG near the focal point of a tightly focused laser beam as a localized microprobe. They also observed some features that were absent in the photograph of linear optical microscope which leads to the concept of SHG microscopy [43].

Gannaway and Shepppard first implemented SHG in scanning optical microscope [44]. They used the 1.064 μm CW laser source which limited the range of specimen. A large input power can only give the effective SHG comparable to the linear optical method. But such high power from CW source may damage the sensitive specimen. Finally the advent of mode-locked laser with very short pulses provided a suitable source for adequate SHG from different types of specimen including poly-crystalline molecular films [45], thin films [46, 47], aluminum [48] and gold[49]surfaces. SHG in biological tissue was first reported by Derr et al. (1965) [50] and Zaret (1965) [51] . Later Fine and Hensen in 1971 reported the details of SHG from corneas, tendon and skin of dog and rabbit at the incident wavelength of 694 nm [52]. SHG was measured in animal tissue like chicken muscle and skin by Guo et al [53, 54, 55]. Biological sample like rat- tail

tendon can also be used as a source of adequate SHG under short pulsed laser source [56].

Many scientists have been working in the study of membrane by the use of such harmonic microscope which may help in measuring inter membrane separation, visualization of membrane potential (Jerome Mertz) [57]. The biological SHG microscopy has been developed to visualize the endogenous tissue structure. The local asymmetry in the specimen along the polarization direction of excitation radiation is an essential condition for generation of second harmonic. Some asymmetries may readily be found in nature in the biological sample. These include helical geometries exhibiting "chirality" as are found in sugar or most amino acids, or on a larger scale, filaments or fibrous bundles. For example, it is well known that collagen, an extracellular protein that is the main fibrous component of skin, bone, tendon, cartilage and teeth can readily be imaged with SHG microscopy (Jerom Mertz).

Guo et al in 1997 [55] and Gauderon et al in 1998 [58] showed that due to quadratic dependence of the SHG on the excitation intensity, three dimensional imaging of SHG is possible The three dimensional second harmonic imaging and structural dependence of SHG may offer a potential non-invasive tool for exploring tissue components and ultimately disease diagnosis [59]. Study is made on SHG from biological tissues and the effect of excitation wavelength on it by Xlaoyuan Deng et al They reported the measurement of SH signals from hyper plastic parenchyma and stroma in malignant human prostrate tissue under femtosecond pulsed illumination in the

wavelength range from 730 to 870nm. The results in these two regions behave differently to a considerable extent and thus provide a possible indicator for identifying tissue components and malignancy.

Depending upon these basic ideas, large numbers of research workers, all over the world are devoting themselves in this field of work to investigate the improvement of scanning probe microscopy. The result of these research works expands its field of utility.

1.3 Proposed Research Work:

Keeping in view of its tremendous utility we have started the research work to design an improved SOM and adaptation of the second harmonic generation on it.

Chapter II contains the complete designing technique of the scanning optical microscope with an improved mode of scanning. We discuss here how it can be improved for better resolution by confocal arrangement, 3-d imaging through z-movement of the objective and also how the second harmonic imaging mode can be adapted. Designing of data acquisition system with its computer software is summarized here so that computerized image can be achieved.

Chapter III is the review of the theoretical part of the scanning optical microscope. It includes the measurement of intensity at the detector for both, type I and type II scanning optical microscope. Resolution measurement for the scanning optical microscope is discussed. Theory of second harmonic generation for plane wave and for Gaussian beam is discussed with its application in SOM. In addition to these, a brief

theoretical idea of signal processing for getting computerized image is mentioned. Moreover, we are concentrating here on modification of a software program for analog to digital conversion (ADC) unit to utilize it in accordance with our purpose for acquiring data.

In chapter IV, we devote ourselves to experimental work so that the designed second harmonic scanning optical microscope (SHSOM) can be used in different practical purposes. Before constructing images we have detected some signals by our conventional SOM and SHSOM. Experiments are performed to verify the second harmonic signal. Conversion efficiency of second harmonic is measured.

The images from different samples show better resolution and better contrast in second harmonic imaging. We have improved the resolution of SOM by using confocal arrangement. We have reported here a method for the measurement of second order non-linear co-efficient from second harmonic images. Some defects, the presence of impurity in crystals and the position of micro crystals are detected. An attempt is made to use the SHSOM as a tool of roughness detection of the surface of a sample. Finally, we have tried to measure the axial resolution of SHSOM and have also achieved the optical sectioning in SHSOM.

Chapter V includes the conclusions drawn from the presented work and a look into the future as regards improved design and application of second harmonic microscope in studying material as well as biological samples.

CHAPTER II

DESIGN AND INSTRUMENTATION OF SCANNING

OPTICAL MICROSCOPE FACILITATING CONFOCAL

AND SECOND HARMONIC IMAGING

2.1 Introduction: Variety of scanning mechanism in microscopy results in different types of scanning microscopy, like far field microscopy, near field microscopy, tunneling microscopy, atomic force microscopy, two photon excited fluorescence microscopy etc. Considering the principle of far field microscopy, the presented SOM is designed. The technology is improved in such a way that the second harmonic mode of imaging can be adapted. In scanning optical microscope, the relative motion between the focused light beam and the specimen can be achieved by two ways (1) by moving the light beam, (2) by moving the object. The presented SOM follows the second principle for achieving this relative motion. The design is further improved to add the z- movement of the focal plane of the objective through the specimen so that optical sectioning can be done [60]- [70].

Different components of the designed SOM can be categorized mainly into three parts:

a) **The vibrating system**

b) **The Optical system**

c) **The electronic system**
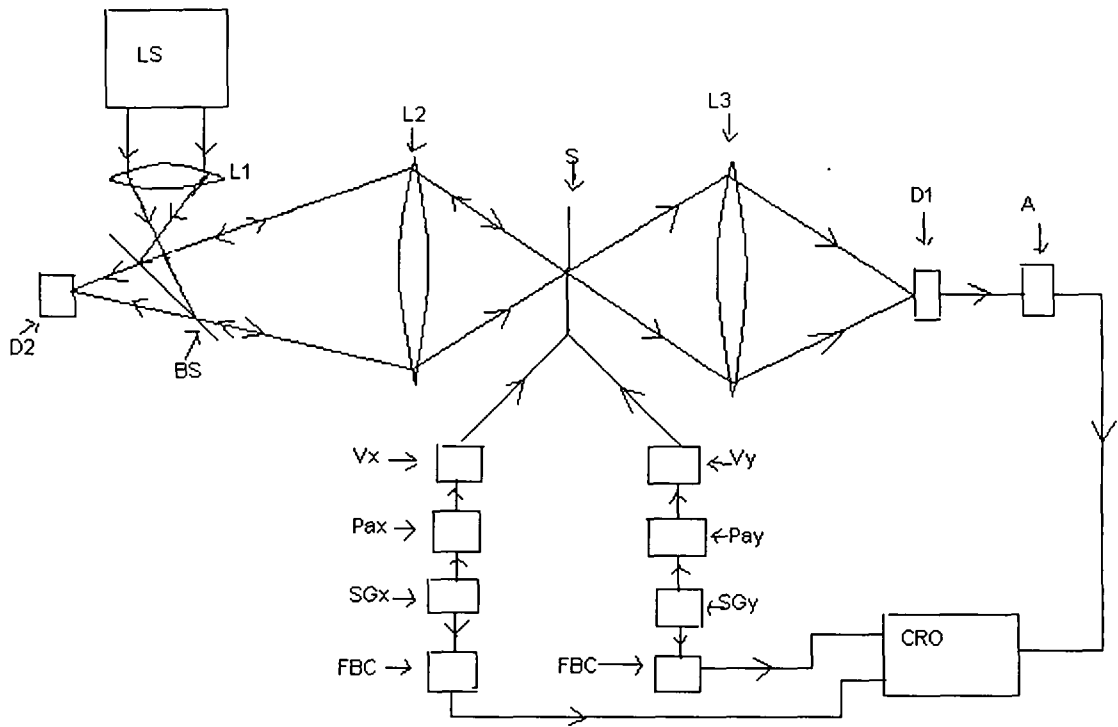
Figure2.1.1Block Diagram of SOM; LS-Laser Source, L1,L2,L3- Lenses, BS-Beam Splitter, S-

Sample Holder, D1, D2- Detector, A- Amplifier, Vx, Vy- Horizontal and Vertical Vibrator, Pax, Pay-

Power amplifier, SGx, SGy- Signal Generator, FBC- Fly-back blanking circuit, CRO as Displaying

unit.
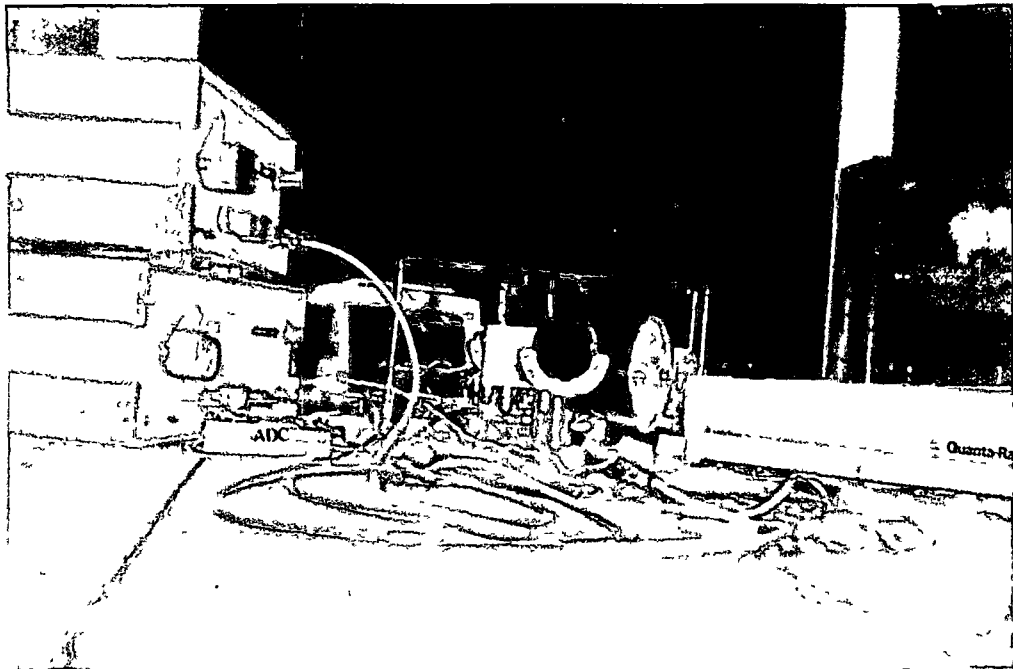
Figure 2.1.2 photograph of the experimental set- up

13

The block diagram of the designed SOM is as shown in the **Figure2.1.1.** The

Figure 2.1.2 shows the photograph of the experimental set up.

2.2. Designing of different parts of SOM in detail:

2.2.a). The vibrating system:

Proper line scanning and frame scanning of a particular area of the sample, similar to the

television picture scanning is an essential condition for getting an image in SOM. So the

vibrating system designed consists of a horizontal and a vertical vibrator which in turn

form the X-Y scanner [71]. Both the vibrators can be designed depending upon the

electro- mechanical method [72] whose principle is same as that of the loud-speaker. A

solenoid of insulated copper is placed inside a cylindrical magnet of diameter 5.5 cm. in

such a way that the coil can vibrate freely when it is energized by a function generator.

The varying current in the form of a saw tooth wave or a square wave from the function

generator passes through the coil and converts temporarily the latter to a magnet. The

polarity of the magnet is changed according to the direction of the current. As a result, the

free end of the coil is attracted and repelled by the permanent magnet causing a vibration.

This vibration is transferred to the sample holder through a light flexible spring

connected at the center of one of the vertical edge (for horizontal vibrator) or at the center

of the lower edge (for vertical vibrator).The sample holder is a rectangular sheet of size

6.5 cm x 5.0 cm made of plastic material. At the center, a hole of radius 1.5 cm is made

which provides the path of light through the sample. The sample with its substrate can be

fixed within a circular ring having two turns. This ring is placed tightly inside a semi

circular wire fitted in the sample holder as shown in the Figure. The ring with the sample can be rotated when needed. In order to restrict the vibration of the object stage only in the x-y direction the other free ends of the holder are supported by stretched spring connected in a rigid support as shown in the **Figure 2.2.1** The variation of amplitude of vibration with applied voltage and frequency response for the x- y scanner are studied and shown by **Figure2.2.2** to **Figure2.2.5.** The frequency response curves are drawn for the applied voltage of 15 volt. Each of these two curves shows a peak around the frequency 800 Hz. This frequency can be considered as the resonance frequency. These curves help in fixing the applied voltage and frequency of the function generator. The line scanning is done in the frequency ranging from 50 Hz to 120 Hz while the frame scanning is done at a slow rate such that more and more scanning line can be obtained in one complete vertical vibration. The complete time for the latter varies from 20 sec to 50 sec. Generally the applied voltage is taken in the lower voltage side (~2.5 volt) as the scanning is done in sample of microscopic size. The scanning length and scanning height over the specimen can be roughly estimated from these four curves. Later on the scanning length is precisely measured by comparing the number of pixel in an image with that of an image of known scanning length.

2.2.b). The optical system :

The performance of the scanning optical microscope depends upon the geometry of the optical system. As far as the type I SOM is concerned, only the aberration of the objective affects image formation. For confocal SOM (type II) the aberration of collector is also important [27]. The scanning probe has to be focused to a diffraction limited spot
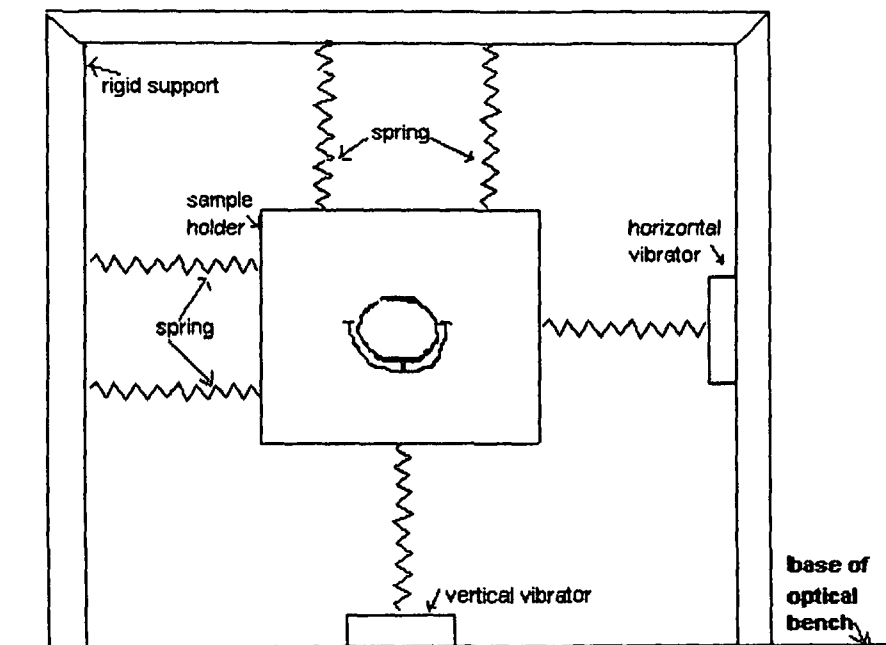
Fig. 2.2.1 Sample holder with vibrating system

amplitude of vibration Vs applied voltage curve for horizontal vibrator
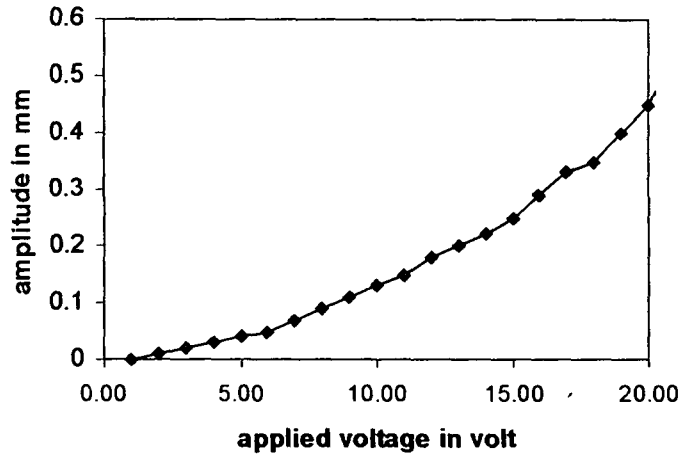
Figure2.2.2

amplitude of vibration vs applied voltage curve for vertical vibrator
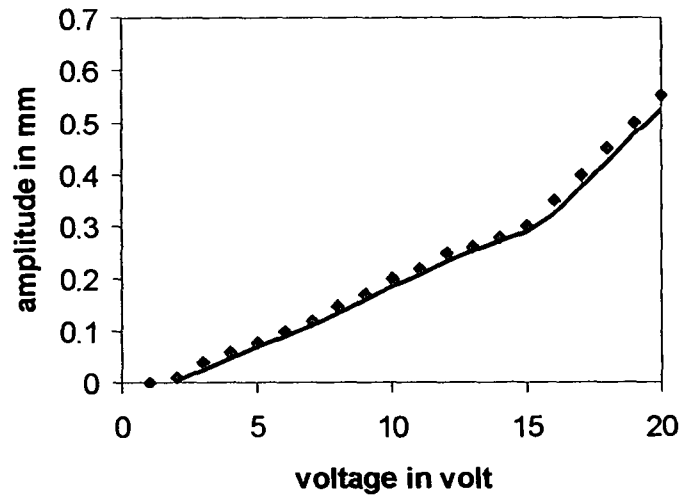
Figure 2.2.3

frequency response curve for horizontal vibrator
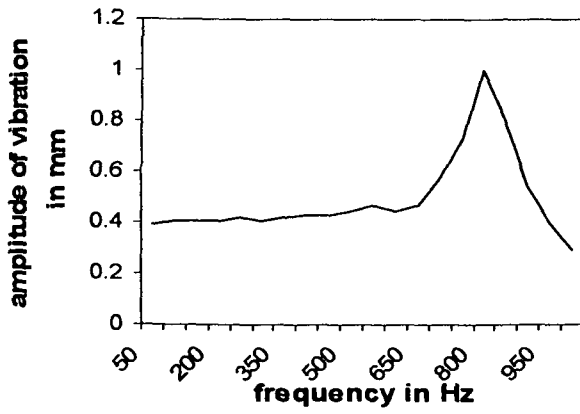
Figure2.2.4

frequency response curve for vertical vibrator

Figure2.2.5

18
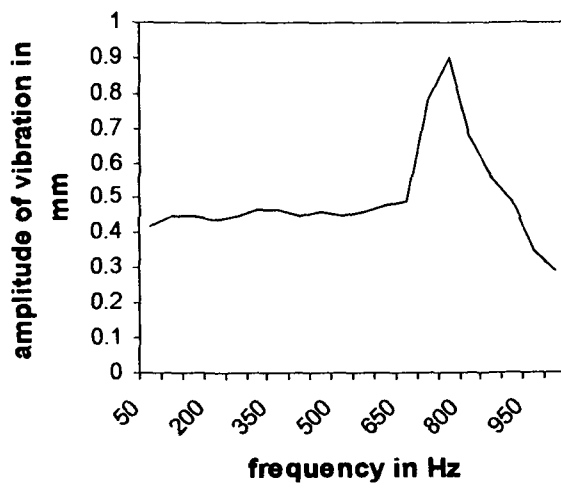
size. The resolution of the microscope is an important feature which depends on the NA of the objective lens. Keeping all these points in view, and also depending upon the type of experiment, the source, focusing lens, objective and collector are selected.

At the initial stage the He- Ne laser source of different average power ranging from 1mw to 30 mw and of wavelength 6328Å are used. For detecting the second harmonic signal high power pulsed laser is more suitable than the CW laser source [73]. An Nd-YAG laser of 1064 nm wavelength serves as a source for this particular case. Some other parameters of this laser source are as follows:

During Q- Switched operation

The resultant pulse width (normal) is < 10 n sec (about 6ns-7 ns)

(fast) is 2.5 n sec

Peak optical power = tens of Mega watt

The pulse triggering sequence and timing (frequency): 10 Hz

In selecting the numerical aperture (NA) of the objective, the following points have to be noticed. To get the high resolution, the NA must be greater according to the

Rayleigh criteria of resolution [74], $D_{min} = \dfrac{0.61\lambda}{N.A}$.

This resolution limit can be overcome by confocal arrangement. For confocal imaging we keep the facility of placing a pin hole in front of the detector both in transmitted and reflected mode of the scanning optical microscope.

On the other hand when the NA becomes greater and greater the angular distribution of the incident beam becomes broader and broader which may decrease the intensity of the second harmonic signal due to the fact that only small portion of the

incident light moving in a particular direction may be matched with the axis of the second order non-linearity [75]. As the non-linear microscopy is the most important goal of this research work, we have selected the objectives with moderate N.A. like 40/0.75 and 40/0.65 air objective in order to find the optimum value of NA.

Over and above these, some other optical components are required for harmonic microscopy. One of them is the appropriate filter for blocking the fundamental light and to allow in passing the SHG signal which depends on the range of wavelength of the incident light. A $CuSO_4$ color glass filter generally known as Russian blue glass is used as a red blocking filter which can effectively block the red fundamental light. $CuSO_4$ solution and also some interference filters are also used for blocking the fundamental wavelength. A half wave plate is used to examine the polarization dependence of SHG signal and a polarizer to determine the polarization of the SHG.

Another important point in any optical system is the proper alignment of the beam. For this purpose, an optical bench is designed along with different mounts for each optical component. For proper alignment of the beam, all mounts are designed in such a way that these can be moved along and perpendicular to the length of the optical bench. Moreover, these can be moved up and down to an adequate amount. **Figure 2.2.6** illustrates the optical bench with its mounts. In order to achieve the Z- scanning through the specimen, a micrometer screw is fitted in the holder for the objective. After getting proper alignment of the beam and proper scanning, the transmitted ray is detected by the photo detector after collecting it by aberration- free collector. Since the incident beam is focused, the SHG is dominantly emitted off-axis. Therefore, to collect entire SHG the NA
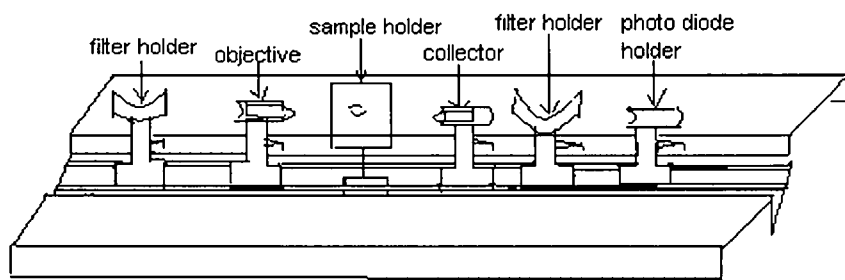
Figure 2.2.6. line diagram of optical bench with its mounts

of the collector must be wide enough [76]. The ratio between the NA of the collector (β) to the NA of the objective (α) determines the nature of illumination i.e if β/α is much greater than 1, the illumination is incoherent while if it is much smaller than 1, it is known as coherent illumination. β/α is approximately equal to unity means partially coherent illumination which is the central point in the theory of conventional microscope. But the imaging of the scanning microscope may be explained without this property [77]. Hence the collector, we have used is of NA, 0.8 (air). However, the objective and collector are sometimes changed according to our purpose of experiment. The same lens which is used as objective can be used as a collector provided the SOM is used in its reflected mode. As our aim is concerned with the detection of the second harmonic signal which is very weak, the detector must be sensitive enough. We use the Til- 81 photo transistor as a detector when the microscope is used as a conventional (type I) scanning optical microscope. Some important parameters of this Til-81 type of detector are tabulated as below:

The electrical characteristics at room temperature (25^0C): [78]

STATIC CHARACTERISTICS:

	Min	Max
Light current (I_l) at V_{ce} = 5 volt	6 mA	....
Dark current(I_d) at V_{ce} = 10 volt		100 mA
Emitter – base breakdown voltage ($V_{(BR)EBO}$)	5V	5V

At I_E = 100 μA , I_C = 0, E_E = 0

Collector – base breakdown voltage ($V_{(BR)CBO}$)   45V   45V

At I_C = 10 mA, I_E = 0, E_E = 0

Collector- emitter breakdown voltage ($V_{(BR)ECO}$)   45 V   45V

(I_C = 10 mA, E_e = 0)

Saturation voltage ($V_{CE(SAT)}$)   0.4V

(I_C = 10 mA, I_B = 1 mA)

DYNAMIC CHARACTERISTICS:

Turn- on time (t_{on})   8 μ sec

(V_{CE} = 10 V, I_C = 2 mA)

Turn- off time (t_{off})   7 μ sec

But it is difficult to distinguish the weak SHG signal from the noise level of the Til- 81

type of photo detector. Therefore, the photomultiplier tube (PMT) is used to detect the

SHG signal. The parameters of the PMT are given below:

INPUT CHARACTERISTICS [79]

Sensitivity of photocathodes   ~ 60 μA/ lumen

Peak response at the wavelength   ~ 500 nm

Recovery time in darkness at room temperature   several minutes to

                                                                         one hour

OUTPUT CHARACTERISTICS

For continuous operation, maximum output current 10^{-5} to 10^{-4} A

23

For pulsed operation	much higher
Load resistor in the anode circuit	$5M\Omega$
Response time	$< 10^{-8}$ sec
Dark current at room temperature	$\sim 10^{-7}$ A

2.2.c). The Electronic system:

The signal detected by the photo detector has to be processed through various electronic circuits to get the final image of a specimen. To construct a magnified image the out put of the photo multiplier tube must be amplified. Since the detected second harmonic signal is very faint, it would require a very good amplification of the signal in order to have reasonable pictures. The following amplifier circuits are designed for different purposes:

The simplest amplifier circuit we have designed is as shown in the **Figure 2.2.7** [80, 81]. This op-amp amplifier circuit is fabricated with fifteen times amplification. The 741 IC, (A, in Figure.2.9) is used in its non-inverting mode. It amplifies the signal detected by the photo detector which is in photo conducting mode. The frequency response curve of the amplifier is as shown in the **Figure.2.2.8** [82]. It works nicely as far as our microscope is a conventional (type I) scanning optical microscope. As it is improved to SHSOM, improvement of the amplifier circuit is needed The trans-impedance amplifier technique can be used to monitor extremely small current. A trans-impedance amplifier circuit can be designed by connecting the photo detector into an op-amps virtual ground input circuit. The circuit is designed by usingOPA111. The photo detector is in its photo conducting mode of operation. Therefore,

24
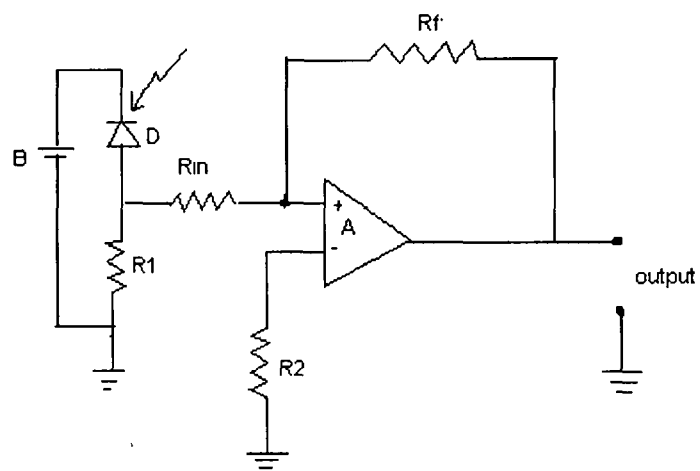
A-741IC,R1- 1K, Rin- 1K, R2- 15 K, Rf - 15 K

Figure 2.2.7 Amplifier Circuit (photo detector in photo conducting mode)

25
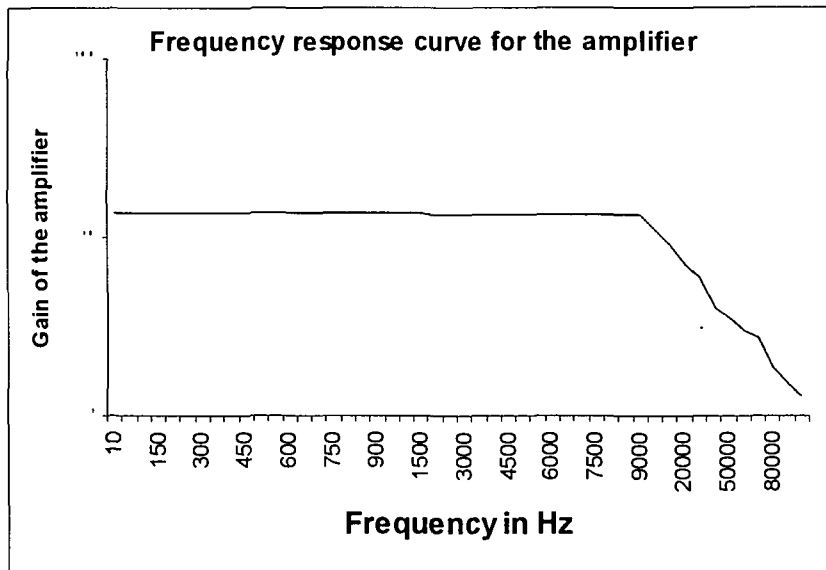
Figure 2.2.8

the current passes from it to the amplifier through the feed-back loop of the amplifier, whose output is a voltage, equal to the input current multiplied by the feed-back resistance. While amplifying very low input current, noise has to be reduced without reducing the usable bandwidth. The out of-band noise can be reduced by inserting a phase compensating op-amp within the main amplifier's closed loop, making a composite amplifier. To allow this composite amplifier to maintain a single phase inversion, it is necessary to reverse the inverting and non-inverting input connections at the main amplifier. The circuit fabricated, is as shown in the **Figure 2.2.9.** At dc and low frequencies the feed-back of the added amplifier is blocked by C2 and the overall open loop gain is the product of both amplifier gains. At higher frequencies, the gain of A2 becomes less than unity resulting in less gain overall than from the main amplifierA1, reducing high frequency noise.

As the scanning spot scans the picture in a raster form, all the picture information has to be blanked out for both the horizontal and vertical retrace time of the square wave used in the function generator for scanning. This retrace time must be as short as possible. Two similar fly- back blanking circuits are designed so that the picture information for the retrace time (for horizontal and vertical scanning) can be blanked out. Two transistors are used for each circuit as shown in the **Figure 2.2.10.** The switching action of the first transistor (T_1) provides the biasing voltage of the second transistor (T_2) which amplifies the actual signal detected by the photo detector. The transistor T_1 is biased in such a way that the positive peak of the square wave has brought it to the cut off
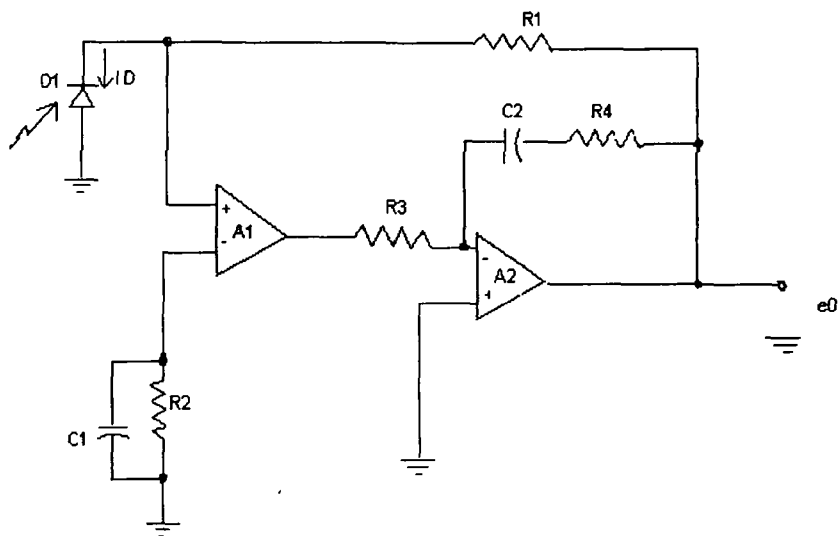
A1, A2- Operational amplifier OPA111   C1 = 0.01 micro farad,   C2 = 0.047 micro farad   R1= 100M ohm ,R2=100M ohm,
R3 = 100Kohm, R4= 1K ohm

Figure 2.2.9 Transimpedance Amplifier (photo detector in photo conducting mode)
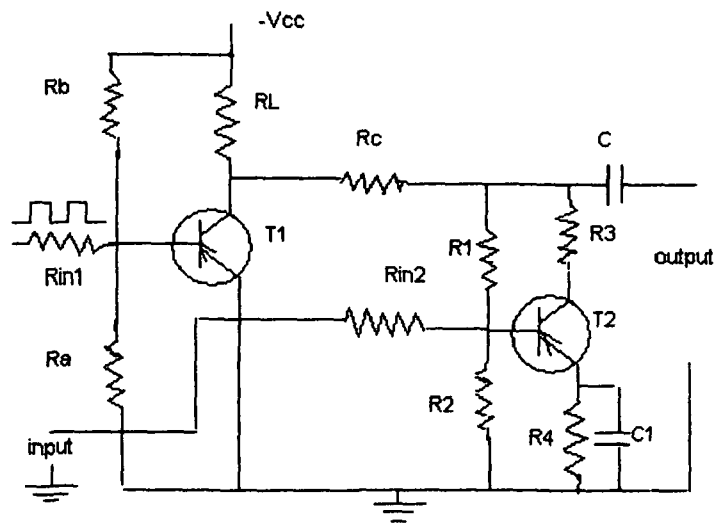
Figure 2.2.10 Fly- Back Blanking Circuit: Rin1- 1K, Ra- 18K, Rb- 75 K, RL- 3.9 K, Rin2-100 Ω, R1-75 K, R2 – 18 K, R3- 1.8K, R4-620 Ω, Rc- 1.2K Vcc- 9 volt (-ve), C- 20 μF, C1- 22 μF

condition. Hence T_1 does not conduct i.e. output can be obtained from T_2. But when the square wave falls to zero which signifies that the retrace in the raster starts, then T_1 is in saturation condition and hence no output can be obtained. T_1 and T_2 are AC 128, Ge p-n-p type transistor with h_{fe} value 175. The supply voltage is 9 volt(-ve voltage). The d.c. load line graph shown in **Figure 2.2.11** gives quiescent collector voltage = 5 volt(-ve).

The resistance $R_3 + R_4 = V_{cc} / I_{c \, max} = 9/ 3.8 = 2.31$ K; nearest preferred value 2.2K.

$$\text{Since } R_4 = \frac{\text{voltage drop across } R_4}{\text{standing collector current}} = 1V/1.65 \text{ A} = 0.606\text{K}; \text{ nearest}$$

preferred value= 620Ω.

Therefore, $R_3 = 2.31$K- 0.606K = 1.704 K; nearest preferred value =1.8 K

The current through R_1 must be at least eleven times the required base current, I_B, where $I_B = I_c / h_{fe} = 1.65$mA (steady collector) / 175 = 9.4 μA

Therefore, current through $R_1 = 11$ x 9.4 μA = 103.4 μA.

Hence $V_{R1} = 9V$- 1.52V = 7.48V (V_{R1} = Bias voltage less the base bias voltage (520mV) and the emitter voltage 1 V).

Therefore, $R_1 = 7.48/ 0.1$ (approx) = 74.8 K; nearest preferred value is 75 K.

Again the current through R_2 will be the current in R_1 less the base current. The voltage across R_2 will be $V_E + V_{BE}$ Using these relations, the value calculated for R_2 becomes 18 K. $R_a = 18$K and $R_b = 75$K are also

Ac128 output characteristics and load line graph
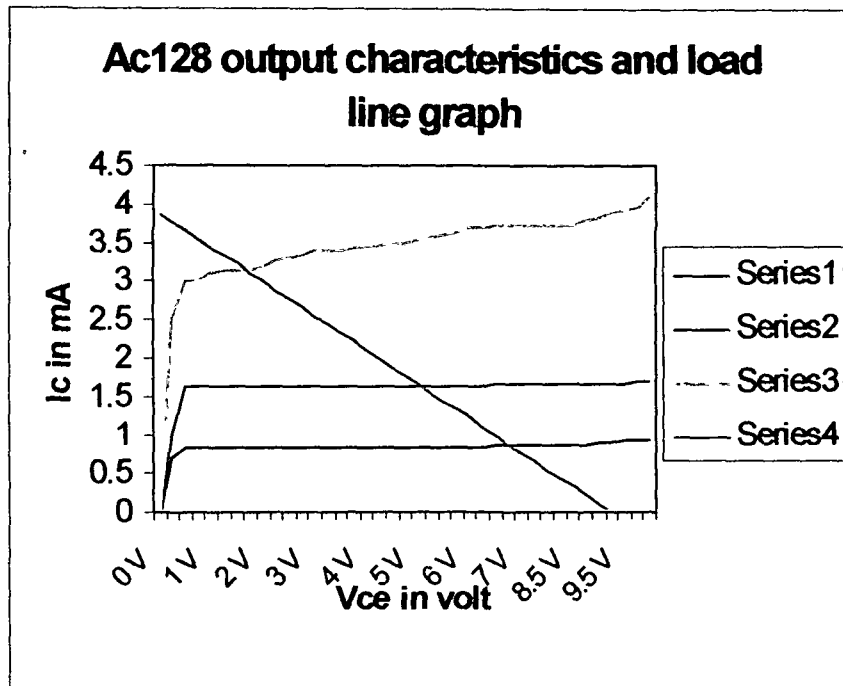
Series1: output characteristics for V_{BE} = 600mV

Series2: output characteristics for V_{BE} = 620mV

Series3: output characteristics for V_{BE} = 640mV

Series4: load line

Figure 2.2.11

used for the transistor T_1 and the voltage of the square wave from the function generator

is adjusted in such a way that switching action of the transistor can be achieved [83]

2.3. Computer Interfacing:

2.3.1. Data Acquisition System:

At the initial attempt though the signals are displayed on the CRO screen, later on

the computer interfacing is done and the images are constructed through the computer

software. For computer interfacing, the analog signal detected by the photo detector and

amplified by the amplifier must be converted to the digital one. For this purpose, one

Data Acquisition system is designed as shown in the **Figure 2.3.1** [84]. This system is

designed using ADC 0809 which is a monolithic CMOS data acquisition device with an

8-bit analogue to digital converter. This 8-channel multiplexer can directly access any of

eight single ended analogue signals. This chip is selected for designing the data

acquisition system due to its high accuracy, high speed, minimal temperature

dependence, minimal power consumption etc. Moreover it is the complete data

acquisition system in itself There are only two external requirements which are the

constant reference voltage at the pin number 12 and a clock. The circuit with op- amp

741 in its voltage follower mode provides the constant voltage with the help of the two

10K resistors, potentiometer P and a zener diode as shown in the **Figure 2.3.1**. The

external clock is provided by 555IC which is working as a free running astable multi

vibrator. Values of resistors R_4, R_5 and capacitor C_3 are such that timer IC produces a

clock about 50 KHz. The data acquisition card along with the two power supplies with

+15 volt output voltage and +5 volt output voltage to supply power to the IC 741 and IC
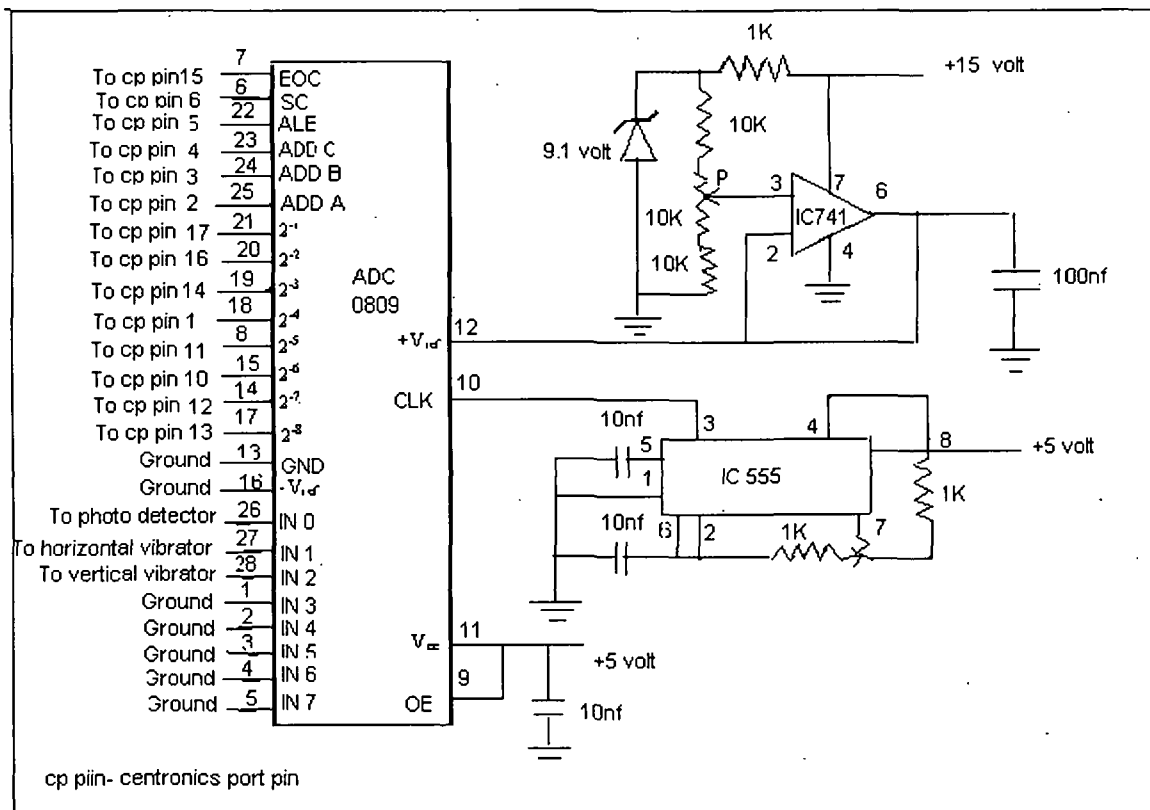
Figure 2.3.1 Data Acquisition System

555 respectively are fabricated on the double sided printed circuit board. Though it is a 8-channel ADC, only 3-input channels are required for our specific experiment. Hence the channels 4 to 8 are grounded. Pin 27 and 28 are used to read the horizontal and vertical vibrator of the scanning optical microscope. The voltage-time signal coming from the photo detector is inserted to the ADC through the input pin 26. For its digital interface with PC, the circuit uses centronics port A flow chart and a simple software are needed to control all the activities of the data acquisition system which are discussed in chapter III.

Power supply circuits required for all these electronic circuits are also fabricated with the main circuit.

2.4.Noise Reduction:

The success of designing a second harmonic scanning optical microscope depends on its noise free condition The external noise like external electro- magnetic wave including visible light, noise due to ground vibration, electric mains ripple, the variation of output power of laser beam due to vibration of laser cavity etc effect the signal detected by the detector which in turn disturbs in getting the actual image of a particular sample. Therefore, many precautions are needed in designing and during the time of experiment such that the over all noise can be minimized to a negligible amount In our set- up, the optical bench is designed by iron plate of thickness 5mm. The base of the holders which hold the optical components like objective, collector, beam- splitter etc. are heavy block of iron of height about 2.5cm. The optical bench is again placed over an iron sheet of thickness 3mm. Thus the disturbance of the ground vibration can be reduced to a

negligible range. The external electro- magnetic wave and light rays may disturb the electronic as well as the optical system of the microscope. All the electronic circuits like amplifier, fly- back blanking circuit, data acquisition system etc are placed inside some boxes made of galvanized iron sheet. The photo detector and the whole SOM system are also covered by sheets of such material so that external light can not reach inside. Moreover the use of co-axial cable for connecting different devices helps in designing a noise free system. The use of stabilized power supply for the laser source and also for other electronic circuits reduces the electric mains ripple. As the second harmonic signal obeys the square law, a small variation in the output power of the laser source results a large change of the second harmonic signal generated in the specimen. By mounting the laser on a vibration free table, both the high frequency and low frequency noise due to the laser cavity vibration can be minimized [85,44].

2.5 Signal detection:

After completion of all these arrangement, the designed SOM is used first to detect some signals from different samples. It is tried to detect the second harmonic signals emitted by optically non-linear material using the microscope. **Figure 2.5.1** and **Figure 2.5.2** show such signals detected by the designed SOM using CRO as the display unit.

2.6 Conclusion: This chapter includes the design consideration of a scanning optical microscope of improved type mainly in three respects such as in mode of

<div align="center">

(a)   **(b)**

</div>

Figure2.5.1 Signal detected by designed SOM on CRO screen, sample ADP crystal (a) typeI

fundamental SOM (b) harmonic SOM
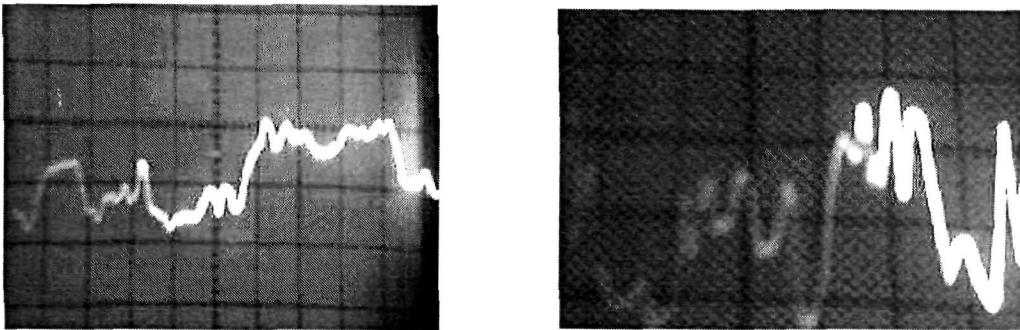
Figure 2.5.2 Second Harmonic Signal detected by designed SHSOM in CRO screen,

Sample: KDP crystal

scanning, second harmonic mode of imaging and in mode of z-scanning in steps. Although the vibrating system in scanning optical microscope was reported earlier, the special arrangement of the system for scanning designed by us as shown in **Figure 2.2.1.** can be cited as an important improvement in our device not reported earlier. The advantage of this system is that it restricts the motion of the sample holder in the X- and Y- direction only, avoiding any tilting motion which is very important for getting the proper image of a particular sample. The rotating arrangement of the sample can also be considered as an important feature of our set-up. In optical system also, we keep the flexibility in using different components so that different types of experiments can be performed. The benefit of the second harmonic mode of imaging is explained elaborately in chapter IV through many experimental results obtained by us. We have added the z-scanning in steps with the help of a micrometer screw fitted in the mount for the objective which may lead us for 3-D imaging.

CHAPTER III

THEORETICAL REVIEW

3.1. Introduction:

The performance of the scanning optical microscope depends on the geometry of the optical system. Depending upon the geometry, it can be divided into two different types: type I and type II or confocal. The type I scanning optical microscope is equivalent to the conventional optical microscope provided the objective lens of both are identical and the collector lens of the scanning optical microscope has the same pupil function with the condenser of the conventional optical microscope. Moreover, the effective source of such a microscope must be infinitesimal which means incident radiation is coherent. In this case, for image formation only the objective lens is important while the collector is used only as a light gathering component. Depending upon the ratio between the numerical aperture of the collector and that of the objective, the imaging property varies from coherent to incoherent through the partially coherent imaging for which β/α ratio becomes approximately 1. But in case of type II scanning optical microscope, the aberrations of both the lenses affect the performance of the microscope. The imaging is similar to that of the incoherent conventional microscope in spite of the coherent incident radiation and coherent detector [27],[77],[86].

3.2. Theory of SOM [87]- [89], [26]:

For the mathematical treatment of this scanning optical microscope, the objective is assumed to be thin and of plane structure so that it may be described by amplitude transmittance function t (x, y). In general this must be assumed complex to account for

39

variations in both absorption and phase changes as a result from changes in optical thickness. The complex object can be represented by the superposition of cosinusoidal gratings of different spatial frequencies and amplitudes. So the spatial frequency content of the object is said to be similar to the frequency content of the electrical waveform. The optical system for imaging modifies input spatial frequency of the object and hence it can be compared with the filter of the electrical waveform. For reflected light microscopy the function t (x, y) represents the amplitude reflectivity; the phase change represents either a phase change on reflection or change in the specimen surface height.

Let us assume that a stationary scanning probe is formed by coherent laser light on the focal plane of the objective of a scanning optical microscope shown in **Figure 3.2**. The raster scanning is done by moving the specimen horizontally and vertically so that point by point image can be built up. This probe formed is actually the impulse response function h (x_0, y_0) of that objective lens. Let t_0 (x_s-x_0, y_s-y_0) be the complex amplitude transmission of the object. Then the amplitude distribution at the detector is given by

$$U_d(x,y) = \int \int_{-\infty}^{+\infty} \frac{1}{j\,\lambda\,d_0} \exp\{\frac{-jk}{d_0}(xx_0 + yy_0)\}P_2(x,y)\exp\{\frac{jk}{2d_0}(x_0^{\,2} + y_0^{\,2})\}$$

$$h(x_0, y_0)t_0(x_s - x_0, y_s - y_0) \qquad (3.2.1)$$

λ is the wavelength of the incident radiation, $P_2(x, y)$ is the pupil function of the detector, d_0 is the distance of the detector from the focal plane and $k=2\pi/\lambda$. If the pupil function P_2 (x, y) of the detector in **Fig3.2.1** is identical to that of the collector lens of **Fig3.2.2** then both the collector system can be considered as identical.
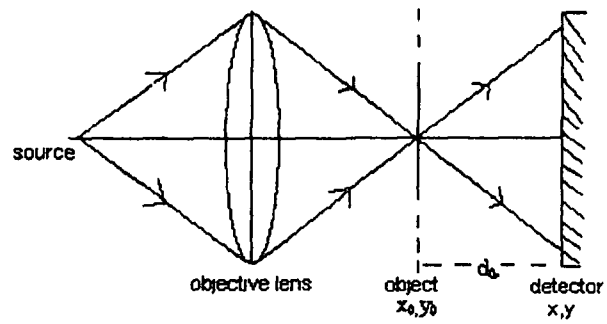
Figure3. 2.1 scanning optical microscope of type I without collector
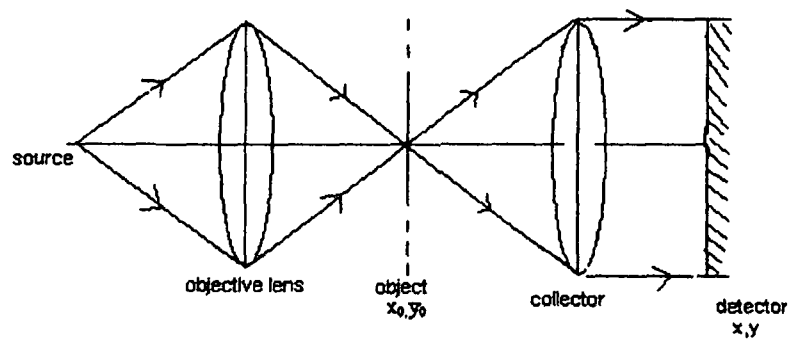
3.2.2- scanning optical microscope of type I with collector

Assuming $\dfrac{x_0}{d_0}, \dfrac{y_0}{d_0} \ll 1$ the total intensity detected by the detector can be expressed as,

$$I_d(x_s, y_s) = const \int\int_{-\infty}^{+\infty} \left| P_2(x,y) \int\int_{-\infty}^{+\infty} t_0(x_s - x_0, y_s - y_0) h_1(x_0, y_0) exp\{\dfrac{-jk}{d_0}(xx_0 + yy_0)\} dx_0 dy_0 \right|^2 dxdy$$

(3.2.2)

and this is allocated to the picture point x_s, y_s

Introducing normalized co-ordinate $u = \dfrac{x}{\lambda d_0}, v = \dfrac{y}{\lambda d_0}$, the expression for intensity

can be written as,

$$I(\lambda d_0 u_s, \lambda d_0 v_s) = const. \int\int\int \int\int \int_{-\infty}^{+\infty} P_2(\lambda d_0 u, \lambda d_0 v) t_0[\lambda d_0(u_s - u_0), \lambda d_0(v_s - v_0)] h_1(\lambda d_0 u_0, \lambda d_0 v_0)$$

$$exp-2\pi j\lambda d_0(uu_0 + vv_0) t_0^*[\lambda d_0(u_s - u_0), \lambda d_0(v_s - v_0)] h_1^*(\lambda d_0 u_0', \lambda d_0 v_0')$$

$$exp2\pi j\lambda d_0(uu_0' + vv_0') dudvdu_0 dv_0 du_0' dv_0'$$

(3.2.3)

42
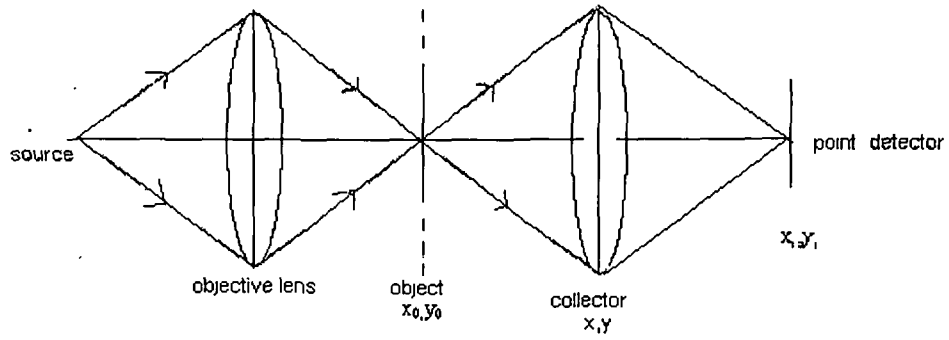
Figure 3.3.1 Scanning Optical Microscope of Type II using point detector
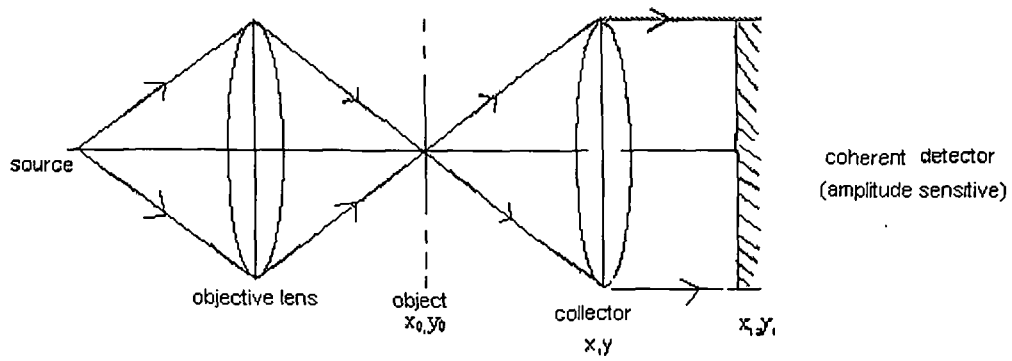
Figure 3.3.2, Scanning Optical Microscope of Type II using coherent detector

43

The amplitude of the signal at the detection plane for a type II scanning optical microscope is given by the expression,

$$V(x_1, y_1) = \int\int_{-\infty}^{+\infty} h_2(x_1, y_1, x_0, y_0) t_0(x_s - x_0, y_s - y_0) h_1(x_0, y_0) dx_0 dy_0 \qquad (3.2.4)$$

where $h_2(x_1, y_1, x_0, y_0)$ is the impulse response of the collector lens. The expression for the impulse response of a thin lens is given by

$$h(x_1, y_1; x_0 y_0) = \frac{1}{\lambda^2 d_0 d_1} exp[\frac{j\pi}{\lambda d_1}(x_1^2 + y_1^2)]$$

$$exp[\frac{j\pi}{\lambda d_0}(x_0^2 + y_0^2)] \int\int P_2(x, y) exp[\frac{j\pi}{\lambda}(\frac{1}{d_1} + \frac{1}{d_0} - \frac{1}{f})(x^2 + y^2)]$$

$$exp\{-j2\pi[(\frac{x_0}{\lambda d_0} + \frac{x_1}{\lambda d_1})x + (\frac{y_0}{\lambda d_0} + \frac{y_1}{\lambda d_1})y]\}dx\ dy \qquad (3.2.5)$$

In type II microscope, a point detector is placed at $x_1 = 0, y_1 = 0$. Further if the lens law $(\frac{1}{d_1} + \frac{1}{d_0} = \frac{1}{f})$ is satisfied and x_0, y_0 are taken to be small.

$$h(0,0; x_0, y_0) = const. \int\int_{-\infty}^{+\infty} P_2(x, y) exp\{-\frac{jk}{d_0}(xx_0 + yy_0)\}dx\ dy \qquad (3.2.6)$$

The signal intensity may be expressed in terms of the function,

$$I(x_s, y_s) = \int\int h_2(x_0, y_0) t_0(x_s - x_0, y_s - y_0) h_1(x_0, y_0) dx_0 dy_0$$

44

$$\iint h_2 {}^*(x_0{}',-y_0{}')t_0{}^*(x_s - x_0)h_1{}^*(x_0{}',y_0{}')dx_0{}'dy_0{}' \tag{3.2.7}$$

3.3. Resolution:

For an object consisting of two equal point objects separated by a normalized

distance $2v_d$ (where $v_d = \pi L(s)$ and s is the ratio between the pupil apertures (a_2/a_1);

known as incoherent parameter) [90], according to the Rayleigh criterion the points are

taken to be just resolved in an incoherent system with circular aperture, when the first

zero in the image of one point coincides with the position of the central peak of the image

of the second point, corresponding to an intensity midway between the points of 0.735

times that at the points. According to the generalized Rayleigh criterion [91] the points

are taken to be just resolved in any optical system if the ratio $\dfrac{I(o)}{I(max)}$ is 0.735, where

$I(o)$, $I(max)$ [92] are the central intensity and maximum intensity respectively. A

similar relation $\dfrac{L(s)\lambda}{a_1/f}$ like the Rayleigh formula $\dfrac{0.61\lambda}{a/f}$ can be written for the separation

between two just resolved points for a scanning optical microscope.

When a beam of light from a He-Ne laser source of wavelength $0.6328\mu m$ is

focused to a diffraction limited spot by an objective of NA 0.65, the resolution calculated

by using $dI = \dfrac{0.61\lambda}{NA}$ gives $dI = 0.594\ \mu m$.

3.4. Theory of Second Harmonic Generation (SHG):

SHG, which belongs to the most important non-linear processes, is an optical

phenomenon of conversion of two photons of same frequency ω to a single photon of

frequency 2ω through an optically non-linear medium having no inversion symmetry. SHG is a three level non-resonant process since the outgoing photon acquires exactly twice the energy of each incoming photon through a virtual state within the specimen. The energy level diagram is as shown in **Figure 3.4.1.** This is an instantaneous process, because, SH photon is generated within a few femto seconds which makes the signal coherent and predominantly emitted in the forward direction [93],[94], [75].

From the electrons which are bound to the atom, non- linear variation of the polarization with the applied radiation field can be expected, provided the radiation field is comparable or greater than the field binding the electrons to the atom. The advent of the high power laser with intense monochromatic radiation makes it possible to get non-linear polarization through interaction with matter. The mathematical expression for total polarization can be given as:

$$P = \varepsilon_0 \chi^{(1)} E + P_{NL} \qquad\qquad (3.4.1)$$

where P_{NL} being the non-linear component of polarization contains the primary non-linear polarization of second order in the electric field and can be expressed as:

$$P_i^{2\omega} = \chi_{ijk}^{2\omega} E_j^{\omega} E_k^{\omega} \qquad\qquad (3.4.2)$$

where $\chi_{ijk}^{2\omega}$ is the second order non-linear susceptibility with the Cartesian co-ordinates denoted by subscript and relevant frequency by superscript. This is a third rank tensor.

Virtual state

ω

Interaction of
two photons
via a virtual
state

Second –
harmonic
2ω

ω

Ground state
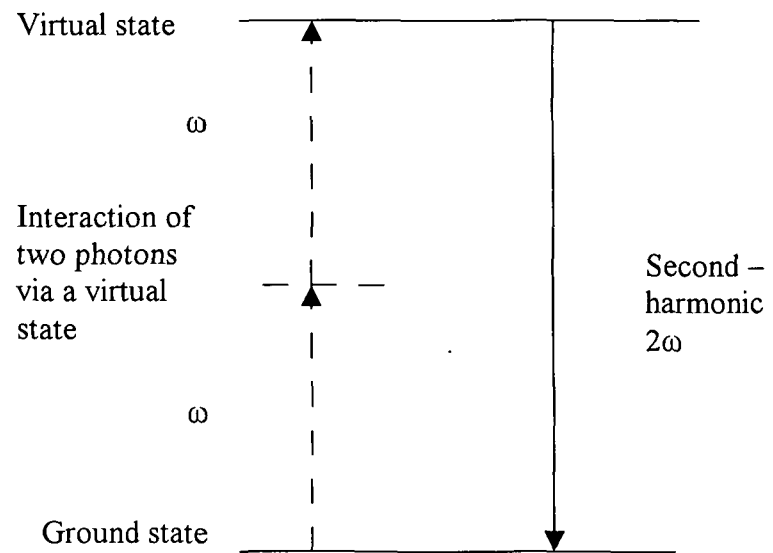
Figure 3.4.1 Energy level diagram of SHG process

E_j^ω, E_k^ω are the electric field component of incident radiation in respective directions as indicated by the subscript.

Assuming that the incident wave representation has the form $E_i \sin \omega t$ the polarization expression **(3.4.2)** can be written as,

$$P_i^{2\omega} = \chi_{ijk}^{2\omega} E_j^\omega E_k^\omega \sin^2 \omega t = \frac{1}{2}\chi_{ijk}^{2\omega} E_j^\omega E_k^\omega (1 - \cos 2\ \omega t) \qquad (3.4.3)$$

In this expression the first term denotes the d.c polarization while the $\cos 2\omega t$ term signifies polarization which oscillates with frequency 2ω exactly twice the incident frequency radiating second harmonic with that of the exciting radiation frequency.

From the symmetry consideration it is found that for a material having inversion symmetry all the tensor element of $\chi_{ijk}^{2\omega}$ vanish which indicates that the SHG will not occurr in centrosymmetric molecule.

Assuming the fundamental incident radiation as a plane wave and using Maxwell's equations the expression for second harmonic intensity can be written as [95],

$$I^{2\omega} = \frac{2\omega^2 d_{eff}^2}{c_0^3 n^{2\omega}(n^\omega)^2}(I^\omega)^2 \frac{\sin^2\left(\Delta kL/2\right)}{\left(\Delta kL/2\right)^2} \qquad (3.4.4)$$

where d_{eff} is the effective second order non-linear co-efficient of the material and it is related to the non-linear susceptibility χ by the relation, $d^n = \chi^n / 2^{(n-1)}$ for second order $n = 2$ and hence $d = \chi/2$. L in equation **(3.4.4)** represents the interaction length

$\Delta k = k_{2\omega} - 2k_\omega$, $n^{2\omega} = \sqrt{\varepsilon_2}$ and $n^\omega = \sqrt{\varepsilon_1}$ are the refractive indices of the medium in SH

and fundamental frequency respectively, $c_0 = 1/\sqrt{\mu_0 \varepsilon_0}$ be the velocity of light in

vacuum. The conversion efficiency can be given as,

$$\frac{P^{(2\omega)}}{P^{(\omega)}} = 8\left(\frac{\mu_0}{\varepsilon_0}\right)^{3/2} \frac{\omega^2 d_{\text{eff}}^2 L^2}{n^{2\omega}\left(n^\omega\right)^2} \frac{P^{(\omega)}}{\text{beam area}} \frac{\sin^2\left(\Delta kL/2\right)}{\left(\Delta kL/2\right)^2} \qquad (3.4.5)$$

3.5. Second Harmonic Generation with Gaussian Beam[96]

The conversion efficiency for a Gaussian beam focused inside a non-linear crystal

can be given by the expression

$$\frac{P^{(2\omega)}}{P^{(\omega)}} = 8\left(\frac{\mu_0}{\varepsilon_0}\right)^{3/2} \frac{\omega^2 d_{\text{eff}}^2 L^2}{(n)^3} \frac{P^{(\omega)}}{\pi W_0^2} \frac{\sin^2\left(\Delta kL/2\right)}{\left(\Delta kL/2\right)^2} \qquad (3.5.1)$$

considering $n^{2\omega} \approx n^\omega$

This is possible only when the crystal length is very much shorter than z_0, the distance at

which the beam cross-sectional area doubles relative to its value at the waist. In such a

case the beam cross-section remains essentially a constant within the crystal and we can

use the plane wave result for electric field. The expression (3.5.1) yields that the increase

of L increases the conversion efficiency. But the conversion efficiency will reduce due to

the increase of beam cross-section with the increase of L. The maximum conversion

efficiency can be expected for focused laser beam with $L = 2z_0 = 2\dfrac{\pi n W_0^2}{\lambda}$ which is

known as confocal focusing L is known as confocal parameter. Hence, $L = k_1 W_0{}^2$, taking

n as unity. Again the diffraction half- angle δ satisfies the relation,

$$\delta = \frac{2W_0}{L} = \frac{2}{W_0 k_1} = \frac{2}{(Lk_1)^{\frac{1}{2}}}.$$

In such a Gaussian beam incident on a non-linear medium, the fundamental electric field can be written as[97],

$$E(x,y,z) = E_0 \frac{1}{1+i\xi} e^{ik_1 z} \exp\left[-\frac{x^2 + y^2}{W_0{}^2(1+i\xi)} \right] \tag{3.5.2}$$

where ξ is the dimensionless co-ordinate, $\xi = \dfrac{2(z-f)}{L}$

From the equation (3.5.2) the second harmonic polarization becomes,

$$P(x,y,z) = P_0 \left[\frac{1}{(1+i\xi)^2} \right] \exp(2ikz) \exp\left[-\frac{2(x^2 + y^2)}{W_0{}^2(1+i\xi)} \right] \tag{3.5.3}$$

which shows the reduction of the effective minimum beam radius from W_0 to $W_0/2$ in second harmonic beam. Hence it results in the reduction of the separation between just resolved points in second harmonic microscope by $\dfrac{1}{\sqrt{2}}$ than that of the conventional scanning optical microscope.

Using Maxwell's wave equation, the second harmonic amplitude collected at a point (x,y,z) when highly convergent Gaussian incident beam passes through non-linear material of thickness $2L = \xi_2 - \xi_1$ can be given by the expression

$$E(x,y,z) = -\frac{i\omega}{2} \exp(2ik_1 z)\sqrt{\frac{\mu_0}{\varepsilon}} \frac{E_0{}^2 d}{1+i\xi} \exp\left\{ -\frac{2(x^2 + y^2)}{W_0{}^2(1+i\xi)} \right\} \frac{L}{2} \int_{\xi_1}^{\xi_2} \frac{d\xi'}{1+i\xi'} \tag{3.5.4}$$

50

Here we assume $\Delta k = 0$; i.e. the index matching condition.

From EE^* the three dimensional intensity expression can be obtained as,

$$I = EE^* = \frac{4\omega^2}{\pi^2}\left(\frac{\mu_0}{\varepsilon}\right)^2 \frac{P(\omega)^2 d^2}{W_0^4(1+\xi)^2}\exp\left\{-\frac{4(x^2+y^2)}{W_0^2(1+\xi^2)}\right\}\frac{L^2}{4}H(\xi_1,\xi_2) \qquad (3.5.5)$$

where,

$$H(\xi_1,\xi_2)$$

$$= \left|\tan^{-1}\xi_2 - \tan^{-1}\xi_1 - \frac{i}{2}\ln\left(1+\xi_2^2\right)+\frac{i}{2}\ln\left(1+\xi_1^2\right)\right|^2$$

$$= \left|\tan^{-1}\xi_2 - \tan^{-1}\xi_1\right|^2 + \frac{1}{4}\left|\ln\frac{1+\xi_1^2}{1+\xi_2^2}\right|^2$$

The expression (3.5.5) for intensity is radially symmetric about the z-axis. This gives the dependence of second harmonic intensity on the thickness of the material also.

The value of W_0 depends on the numerical aperture of the objective by the relation,

$$W_0 = \frac{2\lambda}{\pi NA}$$

Hence for tightly focused beam the reduction of the value of W_0 reduces the confocal parameter L due to its quadratic dependence on W_0. The three dimensional second harmonic intensity expression (3.5.5) also reveals that it depends on the square of the fundamental exciting intensity resulting in sharpening up the point spread function along z-axis This improves the axial resolution of the harmonic microscope over the fundamental SOM similar to the lateral resolution.

3.6 Theory of signal processing [98],[99]:

51

The analog electric signal obtained from the photo detector has to be processed to get the actual image Computerized image is possible only through the digital signal processing. The analog signal can be converted to the digital signal by the use of ADC (analog to digital converter) which performs digitization also known as sampling and quantization. These two are the processes that convert the continuous image irradiance as it is projected by the optical system on to the image plane into a matrix of digital numbers that can be stored and processed by a digital computer.

3.6.1. Sampling:

Let us first discuss about the digitization or sampling. It means the sampling of the gray values at a discrete set of points known as pixel or pel. The cutting of the area into pixels in terms of spatial field of signal intensity is called spatial sampling

Mathematically, digitization is described as the mapping from a continuous function in R^2 onto an array with a finite number of elements:

D

$$g\ (x_1, x_2) \rightarrow G_{m,n} \qquad x_1, x_2 \ \varepsilon \ R \ \text{and} \ m,n \ \varepsilon \ Z \qquad (3.6.1)$$

With numerical differentiation and integration the neighborhood relation is an important operation that is involved in digital signal processing. Neighborhood operations generally combine the gray values in a small neighborhood around a pixel and write the result back to this pixel. This procedure is repeated for all pixels of an image. This operation converts grey scale image into a feature image. It is also termed as filters.

There are two classes of filters, convolution, also termed as linear shift invariant (LSI) filters and rank value filters.

The first characteristic of a neighbourhood operation is the size of the neighbourhood, which is known as the window or filter mask. Most elementary combination of the pixels in a neighbourhood is given by the operation which multiplies each pixel in the range of the filter mask with the corresponding computing factor of the mask, adds up the products and writes the result to the position of the center pixel. This operation is known as discrete convolution and defined as :

$$G'_{mn} = \sum_{m'=-r}^{r} \sum_{n'=-r}^{r} H_{m'n'} G_{m-m',n-n'} = \sum_{m'=-r}^{r} \sum_{n'=-r}^{r} H_{-m',-n'} G_{m+m',n+n'}$$

(3.6.2)

In continuous convolution, the summation of discrete element is replaced by the integration.

3.6.2. Rank Value Filter:

Rank value filters are another class of neighbourhood operations. Here, all pixels in the neighbourhood are not considered to compute the output of the operation 'Comparing and selecting' principle is used. All the gray values of the pixels which lie within the filter mask are arranged in ascending gray value. The median value is sorted out and written back to the center pixel.

Due to the discrete geometry, digitization of a continuous image constitutes an enormous loss of information. Here we reduce the information about the gray values from

an infinite to a finite number of points. So, to get the actual representation of the continuous image by sampled points the following two points must be ensured: (1) no significant information should be lost and (2) no distortion should be introduced. Sampling theorem can help us to formulate the conditions under which the sampled points are a correct and complete representation of the continuous image.

In this theorem the continuous image g (x) is mapped onto the finite matrix $G_{m,n}$ through three separate steps:

1. Image formation; where the influences of optical system, including the sensor is taken into consideration through continuous convolution before sampling the image at certain points of a discrete grid. Mathematically

$$g(x) = \int_{-\infty}^{+\infty} g'(x')h(x - x')d^2x' = g'(x) * h(x)$$ where h(x) be the PSF and the function

g'(x) can be considered as the gray scale image obtained with a perfect sensor i.e. an optical system (including the sensor) whose OTF is identically 1 and whose PSF is a delta function.

2. Sampling; it means that all information is lost except the grid points. Mathematically this constitutes a multiplication with a function which is zero everywhere except for the grid points.

3. Limitation to a finite image matrix; since the sampled image is still infinite in size, it is limited to a finite matrix size by multiplying the sampled image with a box function.

3.6.3. Quantization:

After digitization the pixels still show continuous gray values. In the quantization process these continuous gray values are mapped onto a limited number Q of discrete gray values.

The number of quantization levels in image processing should meet two criteria

First, no gray value steps should be recognized by our visual system and secondly generally a gray level image is quantized into 8-bits.

Thus, a digital image which is a 2-d array of numbers representing intensities of corresponding pixel can be obtained by the use of ADC and computer software. The image processing software MATLAB is used for the construction of images of our experiments after acquiring digital data from the data acquisition system. We have already explained in chapter II about the designing of an ADC circuit (Data acquisition system). The flow chart required for acquiring data using this circuit is as shown in **Figure.3.7.1.**

55

3.7. Flow Chart for Data Acquisition System:

```
                        ( Start )
                            |
                            v
+------------------------------------------------------------+
| Display menu on the monitor screen  Enter a data file      |
| name(FNM) for the particular experiment which will be      |
| stored in the hard disk of the PC  Enter the duration (DUR)|
| for which reading is to be taken in seconds  Enter the gain|
| GA1 of the amplifier in the photo detector unit            |
+------------------------------------------------------------+
                            |
                            v  <--------------- ( B )
+------------------------------------------------------------+
| Pass the address of channel 1 which is connected to the    |
| photo detector to the function(CAL_VOLT) which will acquire|
| the data (VOL1) from the analog-to-digital converter unit  |
+------------------------------------------------------------+
                            |
                            v
             +------------------------------+
             |    Go to and return from     |
             |          CAL-VOLT            |
             +------------------------------+
                            |
                            v
+------------------------------------------------------------+
| Pass the address of channel 2 which is connected to the    |
| square wave driven horizontal i e x-direction vibration    |
| generating unit, to the function (CAL-VOLT) which will     |
| acquire the data (VOL2) from the analog-to-digital         |
| conversion unit                                            |
+------------------------------------------------------------+
                            |
                            v
             +------------------------------+
             |    Go to and return from     |
             |          CAL-VOLT            |
             +------------------------------+
                            |
                            v
+------------------------------------------------------------+
| Pass the address of channel 3 which is connected to the    |
| square wave driven vertical i e y-direction vibration      |
| generating unit, to the function (CAL-VOLT) which will     |
| acquire the data (VOL3) from the analog-to-digital         |
| conversion unit                                            |
+------------------------------------------------------------+
                            |
                            v
             +------------------------------+
             |    Go to and return from     |
             |          CAL-VOLT            |
             +------------------------------+
                            |
                            v
                        ( A )
```

Figure : 3.7.1 Flow Chart for Data Acquisition System

3.8. The C language program for data acquisition system

The C language program corresponding to the flowchart in **Figure.3.6.1** that has been developed for this data acquisition system is given below.

Line Number	Program
1.	#include<stdio.h>
2.	# include<conio.h>
3.	#include<graphics.h>
4.	#include<time.h>
5.	#define REF 5.12
6.	#define LPT1 0x378
7.	int Cal_volt(unsigned char);
8.	void drawline(int *g1, int *oldg1);
9.	main()
10.	{
11.	char add, c, fnm[10];
12.	int g=20, oldg=0, dur;
13.	long x;
14.	float vol1,vol 2, vol 3,
15.	float y0,oldy0=0.0,y1,oldy1=0.0,y2,oldy2=0.0,y3,oldy3=0.0;
16.	FILE *file_ptr;
17.	time_t first, second;
18.	int GraphDriver = DETECT, GraphMode;
19.	initgraph (&GraphDriver, &GraphMode, "c :\ tc\bin\...");
20.	cleardevice();
21.	printf ("\n\nEnter filename :");
22.	scanf ("%s",fnm);
23.	cleardevice();
24.	gotoxy(1,1);
25.	printf("\nduration of reading (in seconds) :");

```
26.     scanf ("%d", &dur);
27.     file_ptr = fopen(fnm, "W");
28.     cleardevice();
29.     drawline(&g,&oldg);
30.     gotoxy(10,24);
31.     printf ("press any key");
32.     c=getch();
33.     gotoxy(10,24);
34.     printf("              ");
35.     first = time (NULL);
36.     while (c!= 27)
37.             {
38.     while (! Kbhit ())
39.         {
40.         vol1 =  REF/ 256) *Cal_volt (1);
41.         vol2 =  REF/ 256) *Cal_volt (2);
42.         vol3 =  REF/ 256) *Cal_volt (3);
43.         fprintf ( file_ptr, "%f,%f,%f\n", vol1,  vol2, vol3);
44.         second = time(NULL);
45.         if(dur <= difftime (second, first))
46.             {
47.             gotoxy (10,24);
48.             printf ("press ESC key");
49.             goto quit;
50.             }
51.         gotoxy(1,12);
52.         printf( "CH:1\n");
53.         printf("vol %1.2f", vol 1);
54.         gotoxy (1,7);
55.         printf ( "CH :2\n");
56.         printf ("vol %1.2f ",vol 2);
57.         gotoxy (1,2);
58.         printf ("CH:3\n");
```

```
59.        printf ("vol %1.2f ",vol 3);
60.        g =g+1;
61.        if (g==639)
62.            drawline (&g,&oldg);
63.        y1=230-(vol 1*15);
64.        line (oldg, oldy1,g, y1);
65.        oldy1=y1;
66.        y2 = 150-(vol 2*15);
67.        line(oldg,oldy2,g,y2);
68.        oldy2=y2;
69.        y3=70-(vol3*15);
70.        line(oldg,oldy3,g,y3);
71.        oldy3=y3;
72.        oldg=g;
73.            }
74.        quit;
75.            ;
76.        c=getch ( );
77.            }
78.    fprintf (file_ptr, "%c %f", NULL, NULL);
79.    fclose(file_ptr);
80.    return (0);
81.    }
82.    cal_volt(unsigned char add)
83.    {
84.        unsigned char bt [8], eoc, ale, stc, out;
85.        int in,x;
86.        ale = 8; stc = 16; eoc = 1;
87.        out = add; outportb (LPT1, out);
88.        out = add | ale; outportb (LPT1,out);
89.        out = out | stc; outportb (LPT1,out);
90.        outportb(LPT1,add);
91.        while(eoc==1)
```

```
92.              {
93.                in=inportb(LPT1+1);
94.                if((in & 8)==0) eoc=0; els eoc=1;
95.              }
96.          while(eoc ==0)
97.          {
98.          in=inportb(LPT1);
99.          if((in & 8)==0) eoc=0; else eoc=1;
100.         }
101.         outport((LPT1+2),0x04); in=inport(LPT1+1);
102.         if((in & 16)==0) bt[0]=0; else bt[0]=1;
103.         if((in & 32)==0) bt[1]=0; else bt[1]=1;
104.         if((in &64)==0) bt[2]=0; else bt [2]=1;
105.         if((in &128)==0) bt[3]=1; else bt[3]=0;
106.         if((in &256)==0) bt[4]=1; else bt[4]=0;
107.         if((in &512)==0) bt[5]=1; else bt[5]=0;
108.         if((in &1024)==0) bt[6]=0; else bt[6]=1;
109.         if((in &2048)==0) bt[7]=1; else bt[7]=0;
110.          in=bt[0]+bt[1]*2+bt[2]*4+bt[3]*8+bt [4]*16+ bt [5]*32+bt[6]*64+bt[7]*128;
111.         return in;
112.      }
113.         void drawline(int *g1, int *oldg1)
114.      {
115.      *g1=70;
116.      *oldg1=70;
117.      cleardevice();
118.      setlinestyle(1,3,1);
119.      line(70,230,640,230);
120.      line(70,150,640,150);
121.      line(70,70,640,70);
122.      line(70,0,640,0);
123.      line(70,0,70,310);
124.      line(639,0,639,310);
```

```
125.       setlinestyle(0,0,1);
126.       return;
127.    }
```

The program is run each time for each sample or for each different position of the sample and different data is acquired. The data recorded is used to get the image through the MATLAB image processing software.

3.8. Conclusion: Thus, chapter III is the review of the theoretical part of the scanning optical microscope and second harmonic generation. Most of these theories are already established but we have studied how to use these in the practical application of our microscope. Moreover, we are concentrating here on modification of a software program for analog to digital conversion (ADC) unit which can be utilized in accordance with our purpose for acquiring data.

CHAPTER IV

COMPARISONAL STUDY OF THE IMAGES OF CONVENTIONAL SOM WITH THOSE OF SHSOM AND CONFOCAL SOM AND SOME APPLICATIONS OF SHSOM

4.1. Introduction:

Very high power density of the scanning spot of the scanning optical microscope due to the use of focused laser light gives rise to second harmonic generation from nonlinear specimen having no centro- symmetricity. Detecting these second harmonic signals and then constructing images of different samples, many properties of the sample can be studied. At the same time, the second harmonic images provide some improvements in finding the contrast and resolution of the scanning optical microscope. As and when the matter of resolution in scanning optical microscope comes up we also need to consider the use of Confocal SOM. This leads us to the detection of signals through confocal arrangement. The images constructed by these signals are compared with the corresponding images of conventional SOM. Such a comparison vividly shows improved resolution in Confocal scanning optical microscope. Various experiments are performed on the above mentioned points and the results thereof are included in this chapter.

4.2. Outline of the experiments:

- 1. Source and specimen selection including sample preparation.

- 2. Detection of scanned signal using conventional SOM and then SHSOM.

- 3. Experiments for confirming SH signal.

- 4. Conversion efficiency Measurement.

- 5. Better contrast of the SH images than the images by conventional SOM.

- 6. Better resolution of SHSOM than that of the conventional SOM. Improved resolution in confocal SOM.

- 7. Measurement of the effective second order non-linear co-efficient of different specimen using SHSOM.

- 8. Study of some crystal defects and presence of impurity inside the crystal.

- 9. Determination of micro crystals.

- 10. SHSOM as a tool of surface roughness detection.

- 11. Axial resolution and Optical sectioning in SHSOM.

4.3. Source and specimen selection [94],[100] including sample preparation:

Second harmonic conversion is characterized by two parameters relating the conversion efficiency, the pump intensity and the non-linear properties of the material. The phase mismatch between the fundamental (exciting beam) and the second harmonic beam also affects the efficiency of SHG. But in case of microscopy, since the thickness of the sample is generally not greater than the coherence length of the sample, the phase matching is not concerned with it. This is also because of the fact that with high

64

resolution as a result of highly convergent radiation, significant second harmonic is generated only in the focal region. The result is that the intensity of the harmonic signal is low. Therefore, in non-linear microscopy, the brightness of the laser beam is very important so that the focused spot attains a very high power density at least of the order of $10^{11}W/m^2$ or more [101]. Use of Q-switched pulsed high power laser as a source satisfies these conditions and hence keeping in view of the availability, Nd-Yag pulsed laser of wavelength 1.064 μm is used as a source for our experiment. The maximum peak power of the laser is tens of megawatt. But it is also a matter of investigation that whether the SH generated by low power laser source can be used for getting a reasonable image in SHSOM. Low power (20mW) He-Ne (cw) laser is used as a source to serve this purpose.

In case of conventional SOM and confocal SOM it is immaterial whether the samples are metal or non- metal, crystalline or non- crystalline. It is also not necessary that the samples are to be non linear or non centro symmetric. But SHSOM prominently can image only non centrosymmetric sample. Therefore we have chosen samples which can meet this requirement of non centrosymmetrycity or surface defects so that meaningful comparison can be made between images of SHSOM and ordinary SOM and also that of confocal and ordinary varity of SOM.

Thus in selection of the sample, importance is attributed on the nonlinear property of the material mainly on the value of the effective second order non-linear coefficient and damage threshold. The absorption of radiation by the material is another property which must be observed for selection of the sample. Lastly, the availability and their costs also control the selection of the sample.

65

KDP and its isomorphs belong to a family of crystals which are very easy to grow from aqueous solution at room temperature and hence easily available. This group of crystal proves to be an important and useful second harmonic generator. From this group we have selected two: KDP (KH_2PO_4) and ADP ($NH_4H_2PO_4$).

The samples are prepared from super saturated aqueous solution keeping separately at room temperature and also inside the refrigerator. The first method takes 7-9 days to grow the crystal of suitable size while the later method gives the same within a few hours. Both the crystals formed by slow evaporation and fast evaporation are used as our samples in different experiments. **Table 4.3.1** illustrates the listed value of non-linear co-efficient, damage threshold, transparency limit (in terms of wavelength) and absorption of these two samples.

Table 4.3.1

Sample	$d_{14}= d_{25} = d_{36}$	Damage threshold (Gw/cm^2)	Transparency In terms of wavelength	Absorption (cm^{-1})
KDP	0.4 to 0.5 pm/V	0.5	$0.22\mu m$ to 1.6 μm	0.005
ADP	0.53 pm/V	0.5	$0.2\mu m$ to 1.2 μm	0.005

Lithium Triborate (LBO) is another second harmonic generator collected for our experiments due to its high optical damage threshold (2.5Gw/cm^2), moderate effective non-linear co-efficient (1.16× 10^{-12}m/V) and its non hygroscopic nature. Absorption is 0.005 cm^{-1}.

An organic crystal urea (NH$_2$)$_2$CO is grown from the super saturated solution in methanol. Its high value of non-linear co-efficient (about 1.4 pm/V which is 2.5 − 3 times larger than that of KDP or ADP), high transparency range from 200 nm to 1.4 µm, high birefringence, high damage threshold as 5Gw/cm^2 at 1.064 µm serve as a very good second harmonic generator but with a drawback of hygroscopic nature.

Many semi conductors like GaAs, ZnSe, CdTe, Te, Zns exhibit high value of non-linearity. Such two samples Te and ZnS are selected to be observed under SHSOM. These two samples are deposited in thin film form, on glass substrate. Te is deposited by thermal evaporation method in high vacuum thin film deposition apparatus while ZnS is deposited by chemical deposition method.

In order to study the presence of surface second harmonic generation (SSHG) [102] Aluminum thin film is used as a sample which is also deposited by thermal evaporation method. Although bulk aluminum has centro symmetrcity, at the surface and at the interface between the two materials, this centro symmetrcity has been broken and hence it is able to generate surface second harmonic.

4.4. Detection of scanned signal using SOM and then SHSOM:

Before going to construct the images of different samples, some experiments are performed in detecting the signals using conventional SOM and then SHSOM which consists of some additional components mainly like some filters and very sensitive amplifier circuit as mentioned in chapter II. Although the signals are initially observed through CRO **(Figure4.4.1, Figure 4.4.2., Figure 4.4.3., Figure 4.4.4)**, finally computerized signals are recorded as depicted as **Figures 4.4.5 and 4.4.6.** These figures illustrate that although there is a similarity between the signals from both the microscopes, the signals from SHSOM show some extra peaks which are not prominent in the signals from conventional SOM. However, some information obtained in the later type is also lost by the SHSOM as clear from the computerized signals.
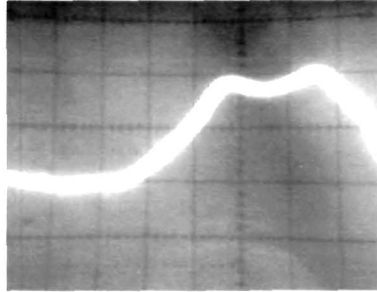
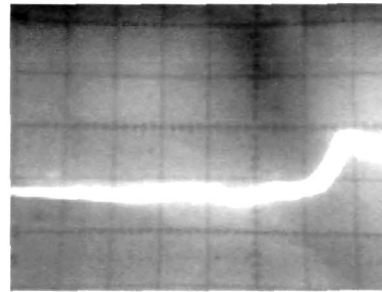**Figure4.4.1. by fundamental SOM**

Figure4.4.2. by SHSOM
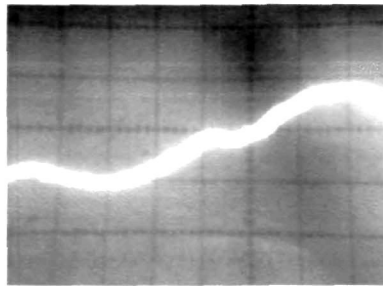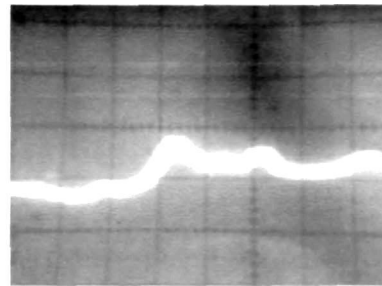

Figure4.4.3. by fundamental SOM
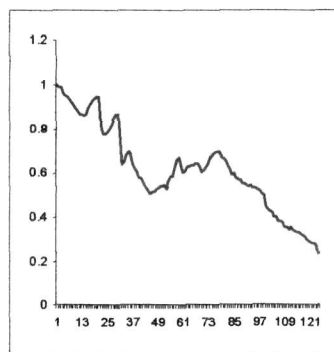
Figure4.4.4. by SHSOM
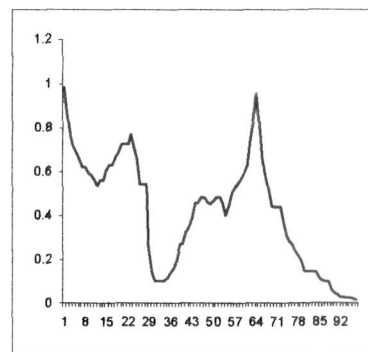

Figure4.4.5 by fundamental SOM

Figure4.4.6 by SHSOM

Fig. 4.4.1- 4.4.6 detected signals from different samples on CRO(4.4.1-4.4.4) and computer monitor(4.4.5&4.4.6)

4.5. Experiments for confirming SH signal:

The weak second harmonic generated at the sample due to the irradiation of strong laser light moves along with this excitation light. Different filters are used to stop the excitation radiation and to pass the second harmonic. But before detecting this signal to get an image, it is necessary to ensure that the signal actually is a second harmonic signal. The $CuSO_4$ solution which is used as a red stopping filter passes radiation from approximately 320 nm to 630 nm. Another narrowband interference filter or a green filter is used so that only the second harmonic wavelength (532 nm) is able to reach the detector when the excitation wavelength is 1064 nm. This is verified by tilting the interference filter. On tilting, the interference condition for that particular wavelength is no longer satisfied resulting in the disappearance of the signal on the detector.

The experiment [52] described below also ensures the SH nature of the signal. In the case of SHG, the harmonic conversion efficiency should decrease monotonically with decreasing laser peak power when all other factors are kept constant.

A theoretical consequence of dependence is that a SH emission pulse should be temporally narrower than the input laser pulse. The temporal pulse width is measured for both incident laser radiation at 1064nm and the same for SH emission at 532 nm (**Figure 4.5.1**).The incident laser pulse has its pulse width at FWHM of about 140 ns. But SH signal gives the FWHM value as 100 ns. As the PMT we have used for detection of the signal has the response time $< 10^{-8}$ sec, we can easily record these pulses. The FWHM of the **Figure4.5.2** illustrates that the SH pulse width is narrower than the former. Thus, this experimental result can be considered as the evidence of SHG from the sample.
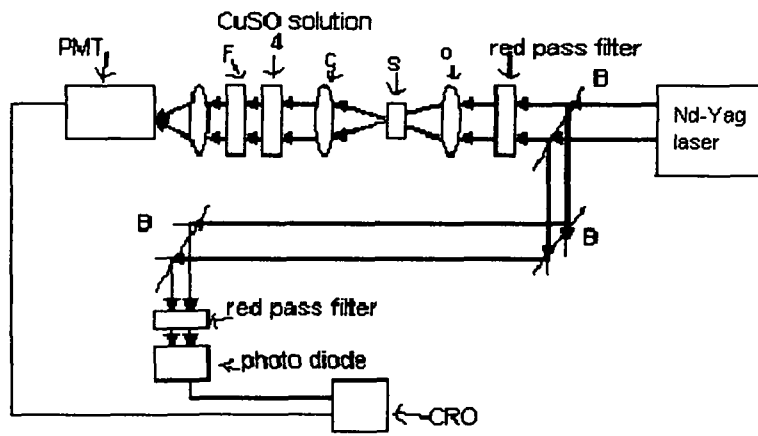
F- Filter , c- collector, s- sample , o- objective , B- beam splitter

Figure 4.5.1 Experimental arrangement for confirmation of SH signal through comparison of

temporal pulse width
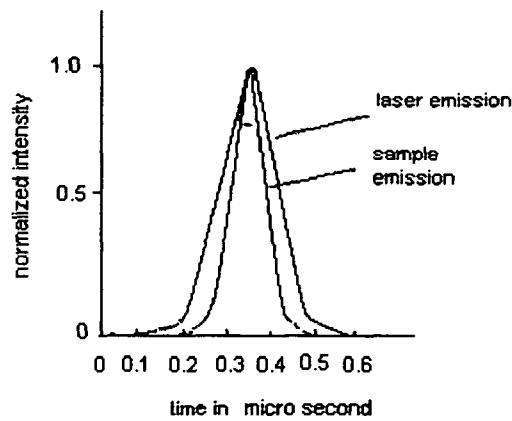
Figure4.5.2 Comparison of temporal pulse width for input laser and SH signal

71

Finally we plot a log SH intensity from LBO sample, against log excitation power as shown in **Figure 4.5.3.** for ensuring the SH nature of the signal in our microscopic arrangement. The source is a He-Ne source of wavelength 6328Å.The **Figure 4.5.3.** shows that the slope of the curve is approximately 2, which proves the quadratic dependence of SH intensity on the excitation intensity[59].

Thus we confirm about the detection of SHG by the photo multiplier tube which is used as a detector of our experimental arrangement.
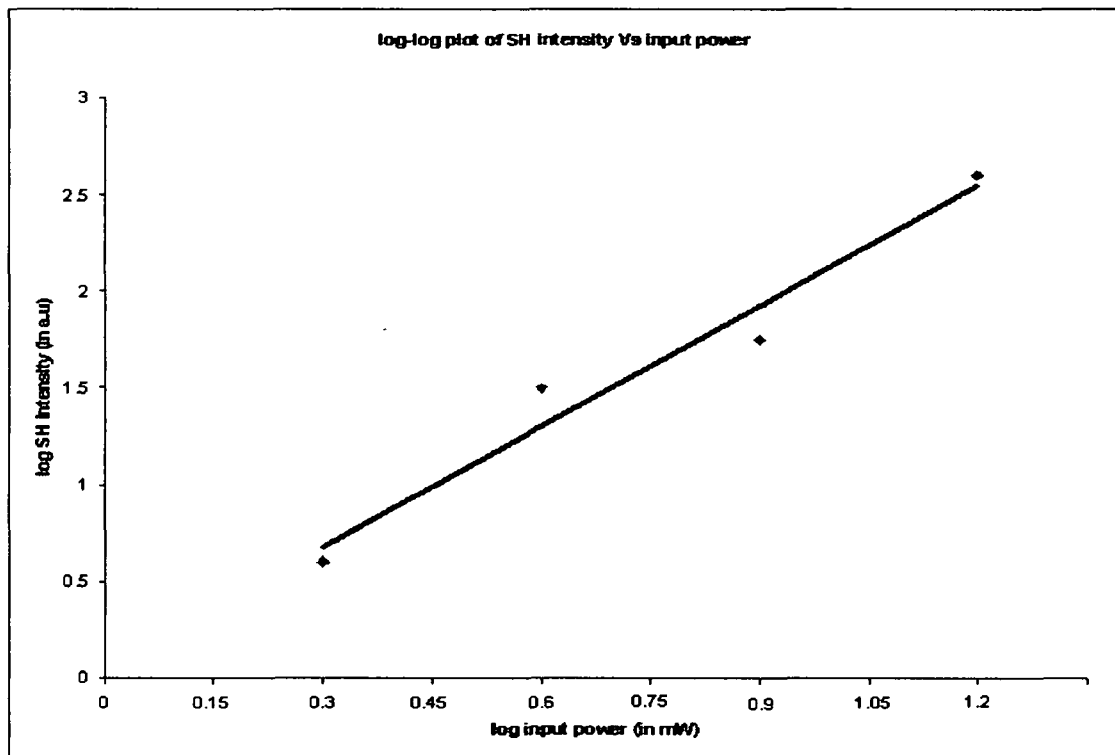
Figure 4.5.3 log SH intensity vs log input power curve

4.6. Conversion efficiency measurement:

4.6.a. Measurement of conversion efficiency i.e. $P_{2\omega}/P_{\omega}$, where $P_{2\omega}$ is the SH power generated while P_{ω} represents the input power of the source, for our microscopic arrangement becomes important due to the dependence of SHG on the input power density and also due to its variation with sample to sample. The input power density can be controlled by the spot size and hence by the N.A. of the objective. The optimization of the later for a microscope is important in getting good images. Considering the focused laser beam as a Gaussian beam, the efficiency can be calculated by using the formula [96],

$$\frac{P_{2\omega}}{P_{\omega}} = 8\left(\frac{\mu_0}{\varepsilon_0}\right)^{3/2} \frac{\omega^2 d^2 L^2}{n^3} \frac{P_{\omega}}{\pi\omega_0^2} \frac{\sin^2\left(\Delta kL/2\right)}{\left(\Delta kL/2\right)^2} \qquad\qquad \textbf{4.6.1}$$

where μ_0, ε_0 are the magnetic permeability and electric permittivity of free space respectively, ω is the frequency of the fundamental beam, d is the effective second order non-linear co-efficient, L be interaction length, $\Delta k = k_{2\omega} - 2k_{\omega}$ is the wave number difference between the fundamental and second harmonic frequency, n is the refractive index of the medium (in phase matching condition $n_{2\omega} = n_{\omega} = n$), wavelength of light used is λ, the radius of the spot $= \omega_0$ Since in microscopy the phase mismatch between the fundamental and the second harmonic can be neglected, we may assume sinc function as unity in equation **4.6.1**. Hence the equation becomes

$$\frac{P_{2\omega}}{P_{\omega}} = 8\left(\frac{\mu_0}{\varepsilon_0}\right)^{3/2} \frac{\omega^2 d^2 L^2}{n^3} \frac{P_{\omega}}{\pi\omega_0^2} \qquad\qquad \textbf{4.6.2}$$

Using a well known SH generator, KDP the conversion efficiency is calculated.

Substituting $\dfrac{2\pi c}{n\lambda}$ for ω, d= 3.6×10^{-24} C/V^2, L= 13×10^{-6}m, (calculated by using the

formula [75], $L = \dfrac{2\pi c}{\omega n_1}\left(\dfrac{n_{2\omega}}{n_\omega} - \cos\theta\right)^{-1}$, for a focused beam, detectable SH is

generated only at the focus, hence the interaction length is very small, the N.A. of the

objective, 0.65 gives the θ value), n= 1.5(approx,), λ= 1.064×10^{-6}m and the radius of

the spot, ω_0= 1.26×10^{-4}m, $\dfrac{P_{2\omega}}{P\omega}$ becomes 0.000007223, with an input power density $2\times$

10^{12}w/m^2= 2×10^8 w/cm^2. Thus the conversion efficiency is 0.0007223%.

4.6.b. Experimental method:

The experimental arrangement is as shown in the **Figure4.6.1.** The focused spot

of laser light of wavelength 1.064×10^{-6}m scans the sample. Both the fundamental light

and the SH produced in the sample are collected by the collector C. Only the SH signal

passes through the filter F which is detected by the PMT.
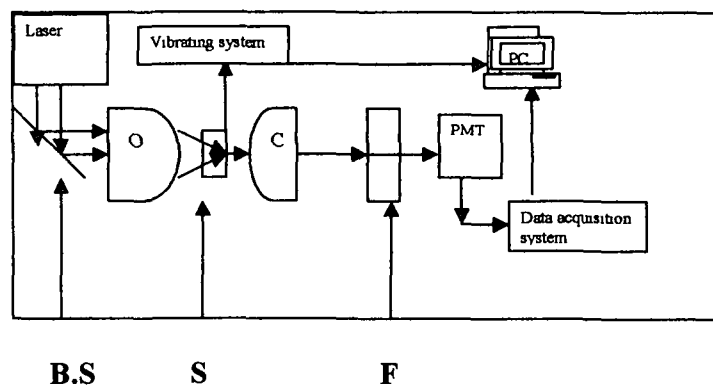

B.S   S   F

Figure 4.6.1. Experimental arrangement for conversion efficiency measurement; B.S- beam splitter,

S- sample in sample holder , F- filter, O- objective, C-collector

The maximum current recorded by the PMT is 3.33×10^{-6}A. At 532 nm wavelength, the efficiency of the PMT is 90% and hence the actual current generated due to SH light is 3.7×10^{-6}A. The absorbed part of the SH light by the specimen is negligibly small for our micron size (20×10^{-6}m) KDP crystal (absorption for KDP = 0.005 cm^{-1}). The load resistance of the photo multiplier tube is $5 \times 10^{6}\,\Omega$. These data along with the input power

10×10^{4}W provides $\dfrac{P_{2\omega}}{P\omega}$ as 0.000006845. So the conversion efficiency is 0.0006845% which agrees well with the calculated value.

Thus the conclusion drawn from this measurement is that the efficiency in such a conversion mechanism where phase matching is not taken into consideration is very low. But very high input power density (in this case power density is 2×10^{12}w/m^{2}) due to focusing provide the sufficient SH intensity required for a reasonable image construction.

4.7 Study of images of different samples

Ensuring the SH signal generated from the sample and calculating the conversion efficiency of the system designed, we proceed to construct images of different scanned samples. From the analysis of these images, many inferences can be drawn as follows:

4.7.1. Better contrast of the SH images [44]:

In the conventional optical microscope, contrast is obtained due to the variations in optical density, optical path length and the refractive index of the sample. On the other hand in case of second harmonic microscope it depends on the ability of generation of SH

75

by the different regions of the sample i.e. spatial variation in SHG within the sample. Again, the second order non-linear susceptibility (χ_2) of the sample is responsible for this SHG. Since χ_2 varies to a large extent in case of different molecular systems of the sample or for different regions within the same sample, the intensity of SH generated at these different regions will also be different resulting in contrast in the SHG images. The absorption of the fundamental and SHG radiation by the sample itself, affect the contrast of which the first is more significant. However, for very thin microscopic sample, the absorption effect is reduced to such an extent that it can be neglected.

We have reported some experimental results which show the achievement of better contrast and super resolution in SHGI in comparison with the conventional scanning optical microscope. Initially we use a low power, CW He-Ne laser source [103] and then pulsed Nd-Yag laser. The schematic diagram of our experimental arrangement is as shown in **Figure4.7.1.1**. The excitation beam from a He-Ne laser of wavelength 6328 Å and of power 20mw is focused through an objective of N.A0.9 into diffraction limited spot. The high numerical aperture is used to increase the power density of the scanned spot and to increase the signal to noise ratio so that low power excitation beam can give us the adequate second harmonic signal for imaging. The X-Y scanning of the sample is done by connecting the sample holder to the electro- mechanical horizontal and vertical vibrators energized by function generators. The N.A of the collector which we have considered is greater than that of the objective which helps in collecting the entire SHG including the dominantly emitted off-axis SHG due to focusing of the excitation beam [104]. The experimental observation proves the N.A. 1.25 of the collector as the

convenient one for our experiment among collectors of N.A. 0.40, 0.65, 0.75 and 1.25.

The red laser light which is transmitted through the specimen is blocked by 'Russian blue

glass' filter and SHG is allowed to pass through a u. v filter. A blue filter is used for

blocking the fundamental light. One u.v blocking filter is used in front of the laser source

so that any u.v generated at the source may not reach up to the specimen. A photo
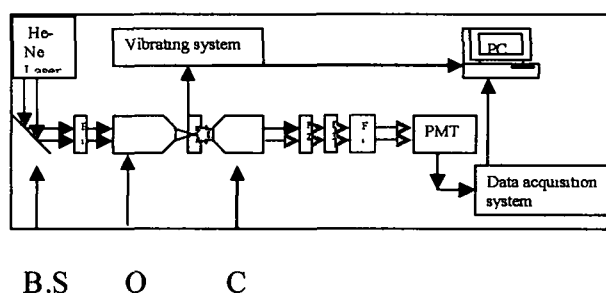

B.S   O   C

Fig. 4.7.1.1 Experimental arrangement for showing better contrast of SHGI B.S – Beam Splitter, O-
Objective, C- Collector, F_1-uv blocking filter, F_2, F_3-Red blocking filter, F_4- u v passing filter

multiplier tube of peak wavelength range of about 300nm-400nm is used as a detector.

These precautions confirm that the signal detected by the PMT is only the SH signal

generated at the specimen. The output signal from the PMT is amplified adequately and

then digitized through a data acquisition system designed by self. The images constructed

by these data are shown in the following Figures.

Experimental Results:

Figure4.7.1.2. represents the image of conventional scanning optical microscope

of LBO crystal of thickness 0.25mm while **Figure 4.7.1.3.** shows the same specimen

scanned under SHSOM. **Figure4.7.1.4** and **Figure 4.7.1.5** are the intensity profile along

an arbitrary line on the images of **Figure4.7.1.2** and **Figure4.7.1.3** respectively. Similarly **Figure4.7.1.6**, **Figure4.7.1.7** are the images for an ADP crystal of 0.5 mm thickness under SOM and SHSOM respectively. **Figure4.7.1.8** and **Figure4.7.1.9** illustrate their intensity profiles. The **Figure4.7.1.2** and **Figure4.7.1.3** may bring another question as to the same sample under the two systems of imaging show some sorts of variation. This can be explained as follows: the detector of conventional SOM detects only the fundamental light as the second harmonic light is very weak in comparison to the fundamental light while the detector of SHSOM detects only the amplified SH signal in which case surface defects and sample non linearity are very important. This leads to the difference in pictures on **Figure4.7.1.2** and **Figure4.7.1.3**. For the same reason **Figure4.7.1.6** and **Figure4.7.1.7** also show some discrepancies in images of the two systems.

Better contrast in SHGI than SOM Image using He-Ne low power source

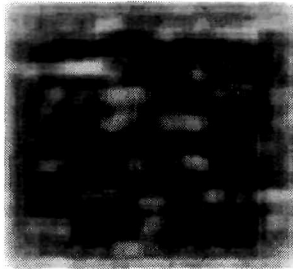Figure 4.7.1.2. Conventional SOM image of LBO
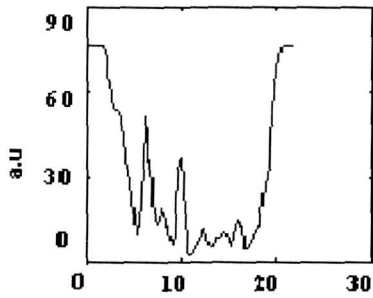

Figure4.7.1.3. SHGI of LBO

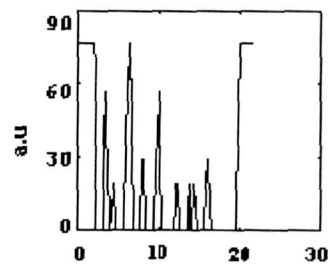Figure 4.7.1.4.Intensity profile of Figure 4.7.1.2

Figure 4.7.1.5 Intensity profile of Figure 4.7.1.3
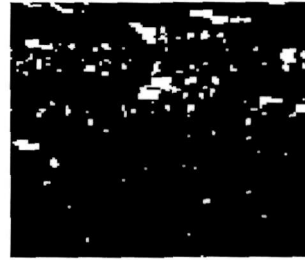
Contd.

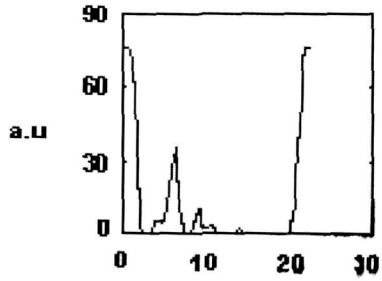**Figure 4.7.1.6 Conventional SOM image of ADP**

Figure4.7.1. 7. SHGI of ADP

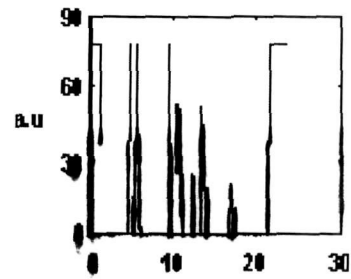**Figure4.7.1.8** Intensity profile of **Figure 4.7.1.6**

Figure4.7.1.9 Intensity profile of Figure 4.7.1.7

80

Although the low power cw laser can be used to construct second harmonic images for some samples having high second order non-linearity under special arrangement, some problems may arise due to the following reasons:

a) Constant heat generation in the sample may damage the sample.

b) Adequate SH signal may not be generated from the sample which has low second order non-linear co-efficient.

c) It may be difficult to distinguish between the noise and the signal during its processing and amplification.

The high power density generated at the focused pulsed laser beam of small pulse-width and high repetition rate can produce significant amount of second harmonic signal instantaneously. Consequently similar experiments are done by using high power pulsed Nd-Yag laser source of 1.064μm with similar experimental arrangement with appropriate objective and filters.

Experimental Results: The images and their intensity profiles along an arbitrary line are as shown in the **Figures4.7.1.10 to Figure4.7.1.13.** From these figures it becomes clear that not only the contrast but also the intensity of the type I SOM is poor enough in comparison to SHGI. Since the crystals like KDP, LBO are transparent in the incident beam of wavelength 1064 nm used for our scanning optical microscope, question arises on the lower intensity of the SOM images. From our study in this respect, we come to the conclusion that the wavelength range for maximum response of the photo detector is responsible for this darkness. We are using the PMT with its maximum response within the wavelength range 500 nm to 600nm and almost blind for the wavelength 1064nm.

Better contrast of

second harmonic image than conventional by using high power Nd- Yag laser and

PMT as detector

Figure4.7.1.10 conventional image of KDP
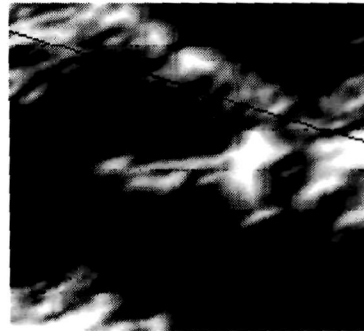
Figure4.7.1.11. SH image of the same sample
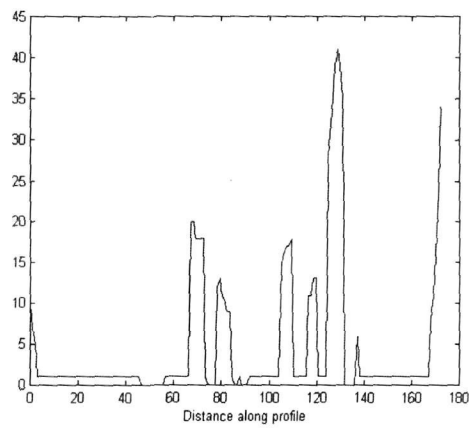
Figure 4.7.1.12 intensity profile of Figure 4.7.1.10
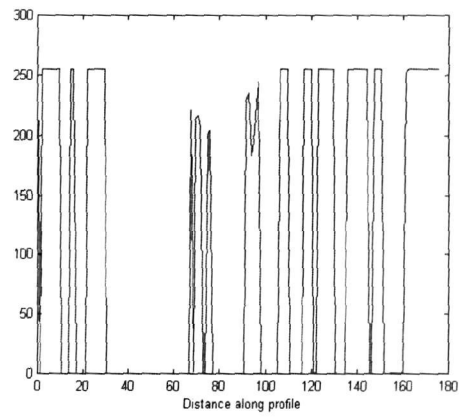
Figure 4.7.1.13 intensity profile of Figure 4.7.1.11

Therefore we have searched out a Silicon photodiode UDT Model PIN-100 which shows the response to the light with wavelength less than 1100 nm. The images with their intensity profiles along an arbitrary line are as shown in **Figure 4.7.1.14** to **Figure 4.7.1.19**. These images along with their intensity profile prove that the contrast in the SHGI is far better than the image of SOM, in spite of the bright intensity of the latter.

These figures prove very well that better contrast has been attained in the SH images than those of the conventional SOM.

Better contrast in SHGI using Silicon photodiode UDT Model PIN-100 as detector and Nd-Yag as source:

Figure 4.7.1.14. SH image of KDP crystal

Figure 4.7.1.15. intensity profile of image 4.7.1.14

Figure 4.7.1.16. SOM image of same KDP crystal

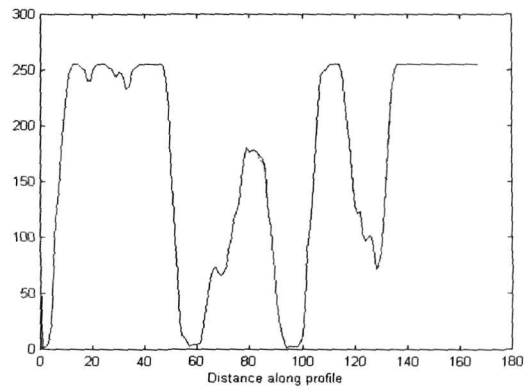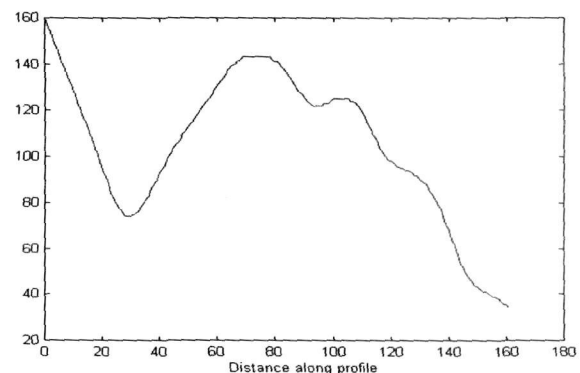Figure 4.7.1.17. intensity profile of Figure4.7.1.16

83
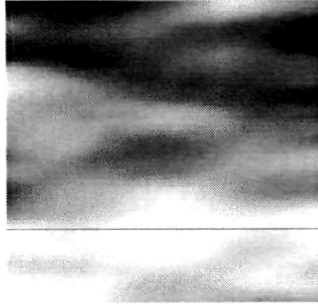
Figure 4.7.1.18.Same image as Figure 4.7.1.16
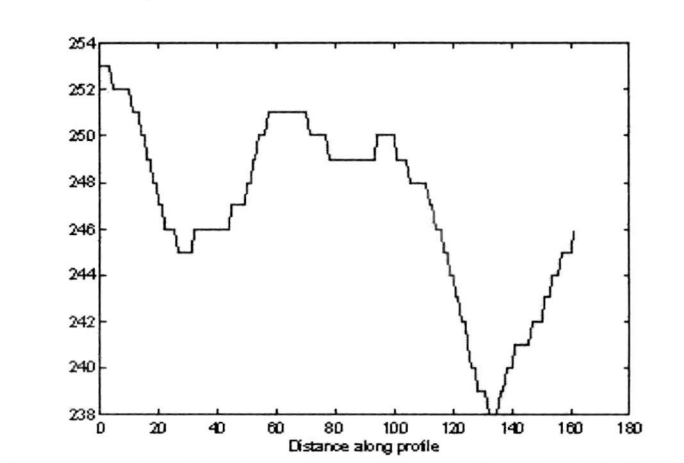
Figure 4.7.1.19. intensity profile of image 4.7.1.18 in intense region along the line shown

84

4.7.2. Better Resolution of SH Image [44],[103]:

The resolution of a microscope is one of the important parameters which depends on the point spread function (PSF) of the objective lens. PSF can be considered as the probability distribution of photon of the laser beam. The increase and decrease of the extent of PSF increases or decreases this probability accordingly. As the SHSOM is one kind of two photon microscope, the quadratic dependence of the SH intensity with that of the fundamental intensity of light decreases the effective spot area within the sample. The effective SH signal originates from the area of each dwell point of the diffraction limited scanning spot which sharpens the spot size by a factor $\sqrt{2}$. Hence the effective radius of the Gaussian SH intensity distribution is reduced by a factor of $\frac{1}{\sqrt{2}}$ of that of the fundamental Gaussian intensity distribution. Hence the Rayleigh criteria of resolution for SH microscope can be written as [75],

$$|d_{min}| = \frac{0.61 \lambda}{\sqrt{2}.N.A} . \qquad 4.7.2.1$$

Hence using same wavelength of light and same N.A of the objective both in SHSOM and conventional SOM, better resolution can be achieved in SHSOM. Thus the violation of Rayleigh criteria of resolution leads to the achievement in super resolution. Some experiments are performed to attain this better resolution in our experimental set-up. Experimental arrangement is same as in **Figure4.7.1.1**

Experimental results:

Figure4.7.2.1 and **Figure4.7.2.2** depict a micro crack in a Tellurium thin film

scanned in conventional SOM and SHSOM respectively using the He- Ne laser source as

mentioned earlier. In **Figure4.7.2.1** the crack can hardly be observed whereas it is

distinct in SHGI in **Figure4.7.2.2**. **Figure4.7.2.3** and **Figure4.7.2.4** are the 2-D intensity

plots of these images. The images shown in **Figure4.7.2.5** and **Figure4.7.2.6** are the

images of a 50μm KDP crystal studied under conventional SOM and SHSOM using the

Nd- Yag pulsed laser source.

All these images along with the images of the section **4.7.1** prove the achievement

in improved resolution in second harmonic scanning optical microscope.

Better resolution of SHGI than Conventional SOM image
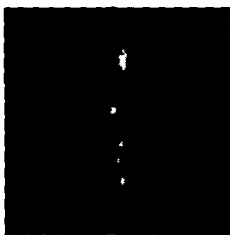
Figure4.7.2.1 SOM image of a micro crack in Te Film

Figure4.7.2.2 SHGI of the same film
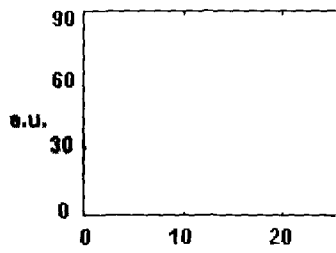
Figure4.7.2.3 intensity profile of Figure4.7.2.1
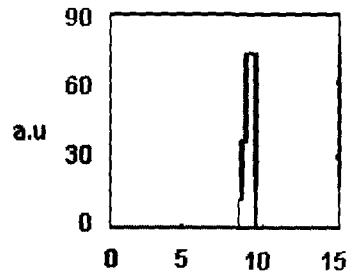
Figure 4.7.2.4. intensity profile of Figure4.7.2,2

contd

Figure4.7.2.5 KDP focused at the edge of the crystal
conventional image

Figure4.7.2.6   SHGI of same sample
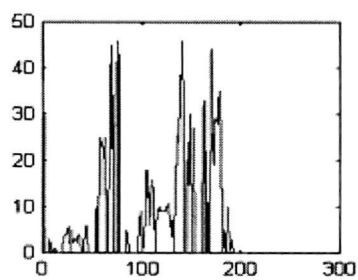
Figure 4.7.2.7 intensity profile of Figure 4.7.2.5
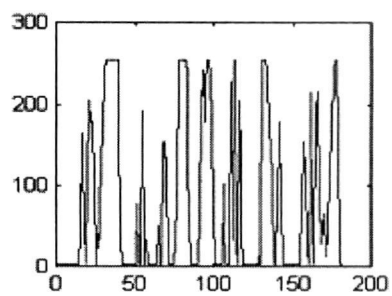
Figure4.7.2.8   intensity profile of Figure 4.7.2.6

4.7.3. Improved resolution in Confocal SOM [26], [27], [101], [114] :

Improved resolution in the scanning optical microscope can be achieved by converting the microscope from type I to type II or confocal. In confocal SOM, not only the point source illuminates a small region but the point detector also collects light only from a small region. The field of view which is decreased due to the use of a point detector in conventional optical microscope is also unimportant in case of scanning optical microscope since in this case the field of view can be increased according to the requirement. The theory of the confocal SOM is discussed briefly in chapter III. We also tried to get the improved resolution by converting our SOM arrangement from type I to type II. For this purpose, we detect the signal from the specimen through the collector lens by using a pin hole in front of the detector. The experimental arrangement is as shown in **Figure4.7.3.1**.
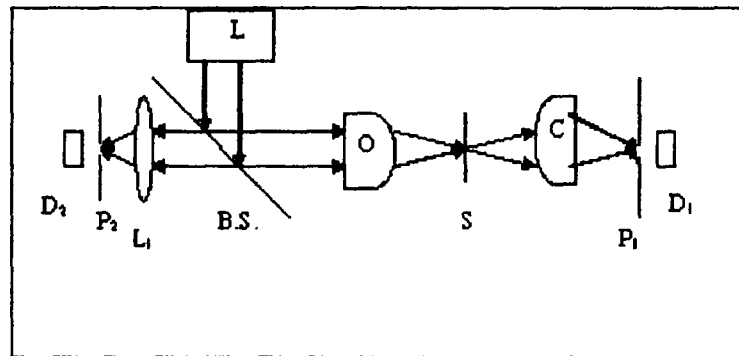
Figure4.7.3.1 Experimental arrangement of confocal SOM (optical part only)

L- He Ne laser, B.S- beam splitter, o- objective, C-collector, s- sample, P_1, P_2- pin holes, D_1,D_2- detectors, L_1- focusing lens

Experimental results: We studied a sample of KDP crystal of thickness about 2mm under conventional and confocal SOM in transmitted mode. The results are as shown in **Figure 4.7.3.2.** and **Figure 4.7.3.3** respectively. One cast iron surface is scanned both under conventional and confocal SOM in their reflected mode and the results found are as shown in **Figure 4.7.3.4.** and **Figure 4.7.3.5** respectively. **Figure 4.7.3.6** and **Figure 4.7.3.7** illustrate the conventional and confocal SOM images respectively of a scratched thin copper film in transmitted mode of the microscope. These images prove that the resolution of confocal SOM is much better than that of the conventional SOM. Thus improved resolution can be achieved with the help of type II SOM.

KDP crystal in transmitted mode

Figure4.7.3.2type I SOM image   Figure4.7.3.3 confocal SOM image

Cast Iron surface in reflected mode

Figure 4.7.3.4 type I SOM image

Figure 4.7.3.5 confocal SOM image

Scratched Copper film on glass substrate in transmitted mode
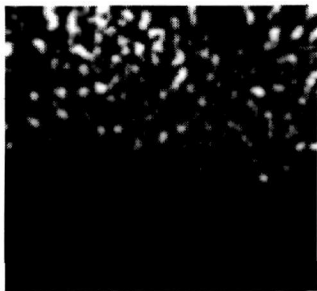
Figure 4.7.3.6 type I SOM image
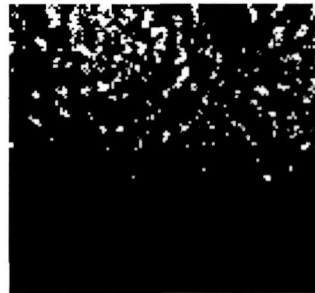
Figure 4.7.3.7 confocal SOM image

Although the improved resolution is achieved in the scanning optical microscope by confocal arrangement it is very difficult to detect very weak second harmonic image signal through the pin hole in front of the detector. As a result second harmonic images can not be constructed. But, as our main goal of this research work is the adaptation of the second harmonic mode of imaging in our designed scanning optical microscope to

study the non-linear specimen hence we performed our other experiments without the confocal arrangement.

4.7.4. Measurement of the effective second order non-linear co-efficient of different specimen using SHSOM:

As the second order non-linear optical susceptibility of the material is responsible for the generation of second harmonic signal in the specimen, it has been attempted to measure the value of effective second order non-linear susceptibility (d_{eff}) by studying the second harmonic intensity generated in the specimen. KDP and urea which are well known second harmonic generators are first used as our specimen to establish the measurement. The samples are embedded in transparent plastic. Experiment shows no second harmonic generation from this substrate. In the next step, we measure the same, for N-(2.Chlorophenyl)- (1-propanamide), a newly synthesized organic non-linear optical material.

Assuming that the absorption of fundamental & SH light is minimal in the object specimen and using plane wave approximation for small length of the sample at the beam waist, the intensity of SHG ($I_{2\omega}$) can be related to the intensity of the excitation light(I_{ω}) by the following relation 4.7.4.1: [95]

$$I_{2\omega} = \frac{2\omega^2 d_{eff}^2}{c^3 n_{2\omega}(n_{\omega})^2}(I_{\omega})^2 L^2 \frac{\sin^2\left(\Delta kL/2\right)}{\left(\Delta kL/2\right)^2} \qquad 4.7.4.1$$

Where d_{eff} is the effective second order nonlinear co-efficient (or non-linear susceptibility), L is the interaction length of the optically nonlinear material, $\Delta k = k_{2\omega} - 2k_{\omega}$ is the wave number difference. For such a frequency conversion phenomenon, the interaction length is an important parameter which represents the length of the crystal upto which the fundamental wave interact usefully with the material. Over this distance the second harmonic light remains in phase with the polarization producing it. Assuming that the microscope objective produces an ideal focus, the interaction length can be written as [75]

$$L = \frac{2\pi c}{\omega n_\omega} \left(\frac{n_{2\omega}}{n_\omega} - \cos \theta \right)^{-1}$$ 4.7.4.2

Where n_ω and $n_{2\omega}$ are the refractive indices of the material for fundamental radiation and second harmonic radiation respectively, θ is the angle made by the direction of propagation of incident beam with the surface normal which can be calculated from the N.A. of the objective.

For microscopy, since the samples are not thicker and since the significant harmonic is generated only in the focal plane of the focused beam, due to the variation of the second harmonic intensity with the variation of the square of the fundamental intensity the phase matching is not concerned with such an experiment [101]. We may assume that within this small distance in which the detectable second harmonic is

generated, the SH is in phase with the fundamental. Therefore, $\dfrac{\sin \Delta k L/2}{\Delta k L/2}$ in equation

4.7.4.1 can be taken as unity assuming there is no phase difference between the exciting

wave and second harmonic wave within the spatial scale of axial resolution. Again the

maximum second harmonic will be generated only for the microcrystal whose orientation

will be aligned with the direction and polarization of the incident beam. Maximum

second harmonic intensity for a particular microcrystal is confirmed by rotating the

sample in our experiment. In equation **4.7.4.1**, $\dfrac{2\pi c}{n \lambda}$ is substituted for ω. Using known

value of other constants, the value of d_{eff} can be calculated provided the second harmonic

intensity ($I_{2\omega}$) generated in the sample can be measured experimentally. For this we

perform some experiments as follows:

The experimental arrangement is as shown in the **Figure4.7.4.1**. Nd-Yag pulsed

laser of 1.064μm wavelength is used in its Q-switched mode. The polarization of the

fundamental light is adjusted by the use of a polarizer (p). Red pass filter stops in case

any second harmonic radiation is present with 1.064 μm. The objective we have used is
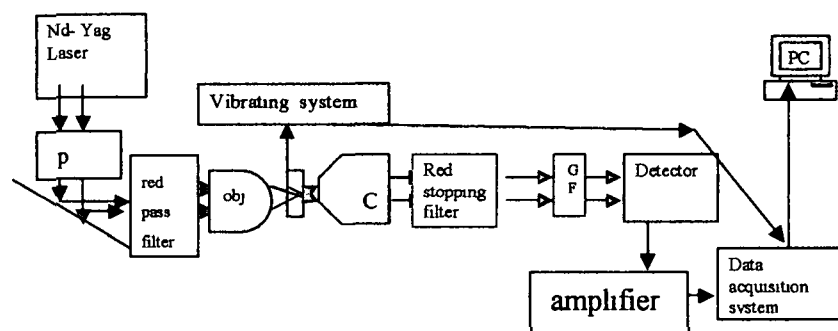
Figure4.7.4.1 Experimental arrangement for d_{eff} measurement

40× 0.65 air objective. The $CuSO_4$ color glass or filter made by $CuSO_4$ solution can stop red light effectively. In our experiment, the later one is used as a red stopping filter to stop the fundamental light from reaching the detector. Another green Filter (GF) is used to pass the green light up to the photo detector. A PMT with its maximum response within the wavelength range 500nm to 600 nm is used as a photo detector. An ADC is used to digitize the data required for constructing images from amplified signals. Intensity profile along different horizontal lines in the region of high SHG can be drawn by image processing software. The maximum pixel point intensities recorded from these images by using MATLAB software are compared with maximum photo currents recorded by the PMT for each image. Calibration of the photo current recorded by the PMT and the intensity of light which generates this current is done before the main experiment. We have obtained a linear relationship between photo current recorded by the PMT and intensity of light, by passing green light of wavelength 532nm (with changing power from 0.05mW to 1 mW) through all optical components kept after the

95

sample of the main experiment as shown in the **Figure4.7.4.1.** and detecting by the same

PMT(each time). Using this linear curve, the data recorded by the PMT each time can be

converted to the intensity of light generated in the sample.

Images of two KDP samples of thickness, 11×10^{-6} m and 12×10^{-6} m and two

urea samples of thickness, 10×10^{-6} m and 11×10^{-6} m with their intensity profiles along

different horizontal lines in the region of high SHG are shown in **Figure4.7.4.2 to**

Figure4.7.4.9.

Figure4.7.4.2 SHG image of KDP embedded in plastic   Figure4.7.4.3 .intensity profile of Figure4. 7.4.2

Figure4.7.4.4. SH I of KDP embedded in plastic   Figure4. 7.4.5 intensity profile of Figure4.7.4.4.
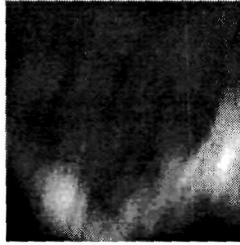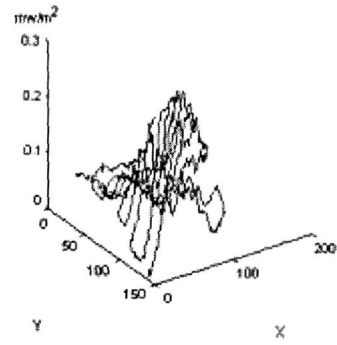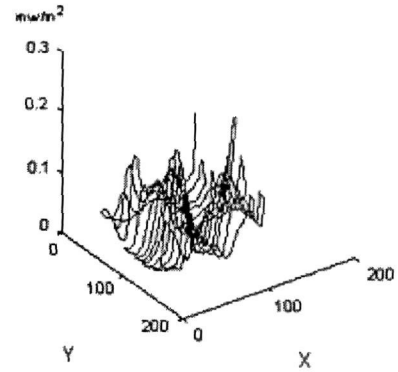

Figure4.7.4.6. SH I of urea embedded in plastic   Figure4.7.4.7. intensity profile of Figure4. 7.4.6.
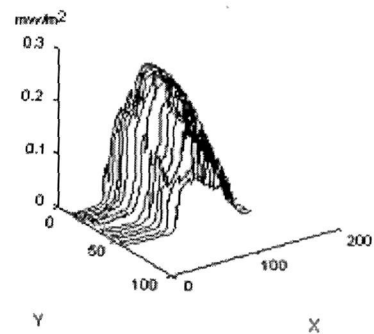
97
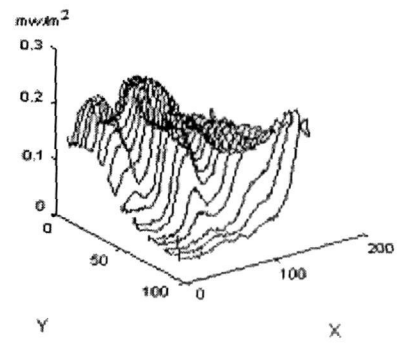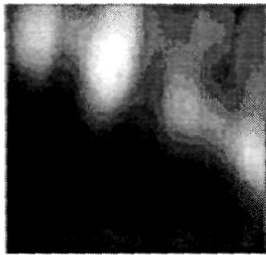
Figure 4.7.4.8. SHI of urea embedded in plastic   Figure4.7.4.9. intensity profile of Figure4.7.4.8.

Calculation of interaction length:

Using equation **4.7.4.2** and substituting the value of $n_1(\omega)$= 1.4939 and $n_2(2\ \omega)$= 1.51 for

KDP [96] and $n_1(\omega)$= 1.4678 and $n_2(2\ \omega)$=1.49(calculated by using Sellmeier equation)

for urea, under the incident radiation of wavelength λ= 1.064 µm, interaction lengths are

found as, $L = 14.595 \times 10^{-6}$ m for KDP and $L = 12.9 \times 10^{-6}$ m for urea. Since the sizes of

the crystals are smaller than the interaction lengths, within which the second harmonic

signals are in phase with the polarization producing it, we may assume that there is no

phase difference between SH and fundamental i. e. Δk= 0. From our experimental curves

it is clear that the maximum SH intensities generated for KDP crystals are 201 µW/ m^2

and 206 µW/ m^2 on the other hand for urea 248 µW/ m^2 and 255 µW/ m^2. Using these

values of $I_{2\omega}$ in equation (1) the result we have found are as :

For KDP (Sample1): $d_{eff} = 0.533 \times 10^{-12}$ m/V, (Sample 2): $d_{eff} = 0.558 \times 10^{-12}$ m/V

For urea (Sample 1): $d_{eff} = 0.66 \times 10^{-12}$ m/V, (Sample 2): $d_{eff} = 0.78 \times 10^{-12}$ m/V

The tabled value of d_{14} for KDP is $0.51 \pm 0.02 \times 10^{-12}$ m / V

While for urea it is about 1.4×10^{-12} m / V.

The contrast in a SH image is obtained due to the variation of ability of the

specimen for producing second harmonic light which in turn depends on the second order

nonlinear co-efficient, d_{eff} . But the value of d_{eff} depends on the molecular structure

mainly the symmetry property, the phase matching condition, the orientation of its

microstructure with respect to both the direction and polarization of the laser beam and

the absorption co- efficient of both the excitation and second harmonic beam. So these

factors effect the contrast variation of the SH image. Already it is explained that we can assume our experiment of microscopic sample with focused beam is in phase matched condition and also the maximum second harmonic can be obtained for the microcrystal whose orientation aligned with the direction and polarization of the incident beam. Therefore, now let us discuss about the effect of symmetry property of the crystal.

KDP and urea belong to the tetragonal system with point group symmetry $\bar{4}2m$. They have only three non-zero co-efficient, d_{14}, d_{25}, d_{36} from second order susceptibility tensor, although the number of independent coefficient is only one under Kleinman symmetry conjecture, in which the nonlinear medium is considered as lossless medium.

Therefore the d_{eff} value which is calculated by the equation (1) will give directly the d_{ij} value. The close proximity of d_{eff} obtained from our experiment with the listed d_{14} value provides a reliable measurement of the first. For the cubic crystal having $\bar{4}2m$ and 23 point group symmetry, non-zero tensor co-efficients are $d_{14} = d_{25} = d_{36}$. Hence the d_{eff} value will give the d_{ij} value also. But, for the crystal symmetry classes having more than one non-zero tensor elements and for absorbing media when Kleinman symmetry does not hold, the polarization of the incident beam has to be adjusted for a particular orientation of the crystal to obtain different d_{ij} values. For different independent non-zero tensor(d_{ij}) components, different independent measurements are to be performed by setting the incident fundamental beam at given polarizations and detecting either s- or p-polarized second harmonic. Formulas for d_{eff} for the various crystal classes and for various optical wave polarizations are available. However, for such crystals, we achieve

the measurement of d_{eff} only and the measurement of different d_{ij} values are yet to be measured.

Some new organic, semi- organic NLO materials such as, N-(2.Chlorophenyl)-(1-propanamide)[105], Glycine Sodium Nitrate [106] etc. have been recently synthesized and optical SHG has also been detected from each of these substances. So the determination of d_{eff} value for such material is also important.

Correspondingly, we have analysed N-(2.Chlorophenyl) - (1-propanamide) with the second harmonic generated from the object specimen as it is scanned. The SH image of that synthesized sample constructed by our SHSOM as shown in the **Figure.4.7.4.10** and **Figure.4.7.4.11** gives the intensity profile. Before detecting the signal for imaging, it is ensured that the signals are actually SH by the temporal pulse measurement technique
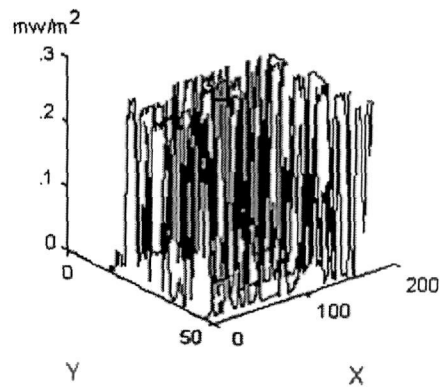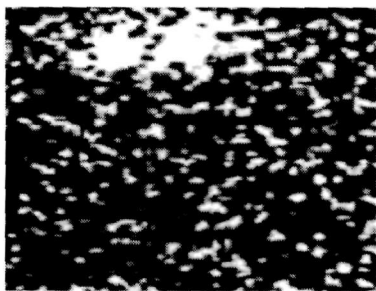
Figure 4.7.4.10. SHGI of N-(2.Chlorophenyl)- (1-propanamide)   Figure 4.7.4.11. intensity profile of Figure 4.7.4.10

as explained in section **4.5.** The maximum SH intensity value with the refractive index$(n_\omega)_x$=1.4639 and $(n_{2\omega})_y$= 1.51 give us the d_{eff} value as 1.3605×10^{-12} m/ V.

In actual calculation the normalization relative to the known (KDP) sample can be carried out so that the d_{eff}^2 varies directly with the SH intensity. It is also confirmed from these measurements that the effective non-linear co-efficient for this new organic material is greater than that of KDP crystal.

Although there are some other methods like Maker fringe measurement, phase matched method etc. for measuring the effective non-linear susceptibility, the method reported here has a great advantage in that no separate phase matching experiment is required. The absorption correction can also be avoided for thin microscopic samples having low absorption co-efficient like KDP(0.005 cm^{-1}). However, problem arises in the measurement of different dij values for the crystals having more than one non-zero tensor elements.

4.7.5. Study of some crystal defects and presence of impurity inside the crystal:

A perfect crystal with regular arrangement of atoms can not exist. There are always defects in the crystals [107].

Three basic classes of defects in crystals are:

1. Point defects- atoms missing or in irregular places in the lattice (lattice vacancies, substitutional and interstitial impurities, self-interstitials).

102

2. Linear defects- group of atoms in irregular positions (e.g. screw and edge dislocations).

3. Planar defects- the interfaces between homogeneous regions of the material (grain boundaries, stacking faults, external surfaces).

We have attempted to detect some crystal defects of crystal by studying SH images recorded by our microscope in transmission mode. The experimental arrangement is same as shown in **Figure4.7.4.1**.

Experimental Results:

The samples studied are single crystal of urea with the size of $50\mu m$ and a single crystal of KDP (63 μm). The following are some such images: In **Figure4.7.5.1** it is observed that there are some dark spots at the positions A, B and C in the bright back ground. The size of these spots are studied from the point of resolution and found that these are of $3-5\mu m$. Hence it can be attributed that the spots appeared due to substitution of the urea atoms by some other atoms so that no SH is generated from them indicating point defects of the crystal. At the position D also, a black region appears

which confirms the absence of SH intensity. This is due to the presence of some impurity inside the urea crystal such that the foreign material has inversion symmetry and hence lacks of second order non-linear co-efficient. Again in **Figure4.7.5.2** one dark line
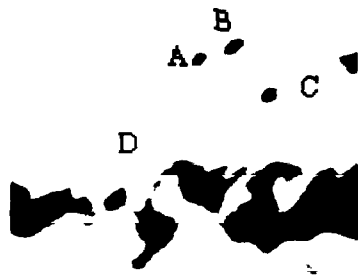
Figure 4.7.5.1.point defect and presence of impurity in urea crystal
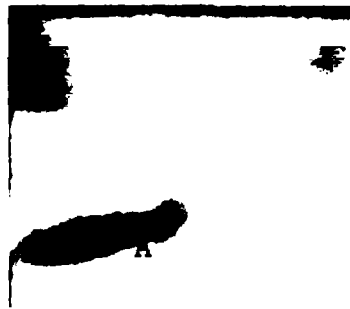
Figure4. 7.5.2 dislocations in KDP crystal

appears at A. This may indicate that the edge dislocation of the crystal occurs due to the extra lattice plane inserted in the crystal upto a certain distance. The insertion of this extra lattice plane will disturb the original symmetry property of the crystal and also the crystal orientation. As a result the variation of the second order non-linear co-efficient may occur within the crystal which gives rise to a variation of second harmonic intensity generated in the crystal.

4.7.6. Detection of microcrystal:

The position of nonlinear micro crystals grown over a substrate can be detected by studying the second harmonic image [58]. Urea is grown over a rough transparent plastic material. After deposition of the crystal, some crystals are removed by rubbing gently over it.

Experimental Results:

The image is taken under the SHSOM which is shown in the **Figure4.7.6.1.** Second harmonic is generated only when light passes through urea crystal but not through the other portion of the substrate. The bright positions (A to F) of the **figure4.7.6.1** indicate the positions of urea microcrystals whose orientation coincide with the direction and polarization of the incident beam. Similar microcrystals of LBO are shown in **Figure4.7.6.2.**
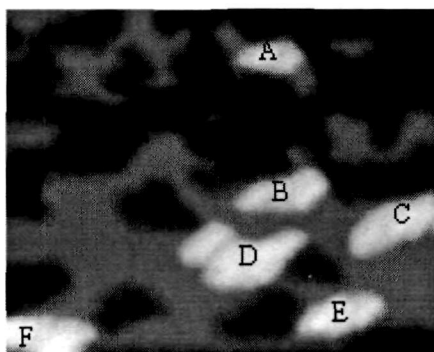
Figure 4.7.6.1.microcrystal of urea deposited in plastic material

Figure4.7.6.2 microcrystal of LBO in plastic material

4.7.7. SHSOM as a tool of roughness detection:

At the interface between two materials or on the surface of a material, the inversion symmetry is broken and hence it behaves like a non centro-symmetric substance from which second harmonic generation is produced. This surface- enhanced second harmonic generation (SESHG) can be used as a tool for probing surfaces and interfaces since only the first few atomic or molecular mono layers on either side of the interface take part in breaking the centro symmetricity[108]. The intensity of this process at the surface is enhanced by many orders of magnitude at rough metal or semi-conductor surfaces.

The equation for the second harmonic intensity I (2ω) from an interface in either reflection or transmission geometry, derived by Heinz [109], Mizrahi and Sipe [110] is given as

$$I(2\omega) = \frac{32\pi^3\omega^3 \sec^2\theta_{2\omega}}{c^3} \left| e(2\omega).\chi^{(2)} \cdot e(\omega)e(\omega) \right|^2 I^2(\omega)$$

4.7.7.1

Where $\theta_{2\omega}$ is the angle from the surface normal at which the S.H.G. signal occurs, the vector $e(\omega)$ and $e(2\omega)$ describes the fundamental and second harmonic light fields at the surfaces and all other symbols have their usual meaning. From this equation, it is clear that the intensity of the SESHG is proportional to the square of the fundamental intensity. It also varies as the square of the surface non-linear susceptibility $\chi^{(2)}$. The idea of SESHG can be implemented in scanning optical microscopy [43],[111]. This type of microscopy becomes very attractive due to the possibility of probing electro dynamics at rough surfaces and hence providing a technique for surface studies [112].

The location of bump or groove is attempted to be determined by studying the SESHG intensity of the sample. The surface second harmonic signal for a particular horizontal line (without using the vertical vibrator) in the second harmonic scanning optical microscope (far field, conventional) has been detected. These signals are compared with the topographic signals detected by the scanning optical microscope through the phase shifting interferometric method [99] for the same line. The phase shifting is done by shifting the focal plane of the objective which is placed over a mount fitted with micrometer screw.

We have studied the SESHG from Aluminum (metal) film and a semi-conductor Tellurium film on polished glass substrate. Aluminum is a centro symmetric material whereas Tellurium has no centro symmetricity and SH signal can be generated from the bulk material also.

The experimental arrangement is as illustrated in **Figure.4.7.7.1**. An Nd-YAG pulsed laser of wavelength 1064nm with a frequency of 10Hz and of pulse width <10ns is used as a source of light in the second harmonic scanning optical microscope. The microscope is used in its reflection mode. The incident beam is focused on the surface of the specimen using an objective of N.A. 0.65. The specimen is scanned in two dimensions in raster form repeatedly. The surface second harmonic signals along with the fundamental light reflected from the sample are collected by the same objective. The SH signals are then separated out from the excitation beam using a narrow band pass interference filter. The filtered signals are detected by PMT to construct SH image. Then

the vertical vibrator is switched off so that SH signal for a particular horizontal line can

be detected to give the SH intensity profile for that line. After that the filter and amplifier

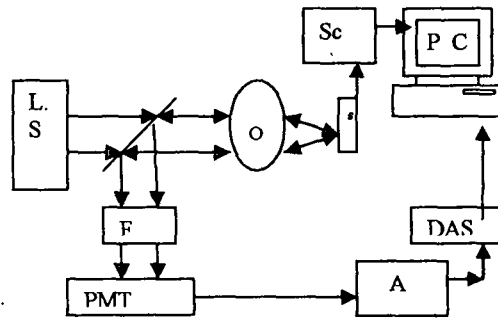Figure4.7.7.1.scanning optical microscope in reflection mode. LS- laser source,

O- objective, s- sample, F- filter, A- amplifier, DAS-data acquisition system, Sc X-Y scanner
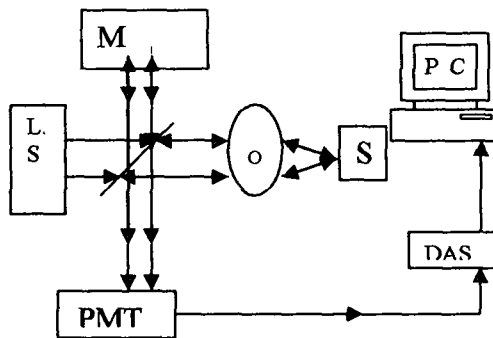
Figure4.7.7. 2.Experimental arrangement for phase shifting interferometry.

are removed and an optically flat mirror is inserted as shown in the Figure 4.7.7.2 in such

a way that other components along with the object specimen is not disturbed. Now the

resultant intensity of the two interfered beam (object beam reflected from the specimen and reference beam reflected from the mirror) is recorded for the same horizontal line mentioned above to get the surface profile for the line by phase shifting interferometric method where the intensity at a particular point (x, y) can be written as

$$I(x, y) = I_0 + I' \cos[\varphi(x, y) + \varphi(t)]$$

where $\varphi(x, y) = \tan^{-1}\left[\dfrac{I_3 - I_2}{I_1 - I_2}\right]$; I_1, I_2 and I_3 are intensity values at the point (x, y) for

three different phase differences of $\varphi(t) = 0$, $\pi/2$ and π respectively. So, the surface height map can be obtained by using the equation $h(x, y) = (\lambda/4\pi) \varphi (x, y)$ (assuming low numerical aperture of the objective) along with the use of the phase − intensity graph as shown in **Figure4.7.7.3**.

Experimental Results and Discussion: **Figure.4.7.7.4** and **Figure.4.7.7.5** show SH images of Al and Te thin film respectively. **Figure 4.7.7.6** and **Figure 4.7.7.7** are intensity profiles for Al and Te sample for two particular horizontal lines respectively. **Figure 4.7.7.8** and **Figure4.7.7.9** illustrate the topography of Al film and the topography of Te film respectively drawn by the data of phase − shifting interferometry experiments for the same horizontal lines. These diagrams describe the dependence of SH intensity with the roughness of the surface. The SESHG can be considered as the cause of this dependence, since this type of enhancement of SHG depends on the roughness of the
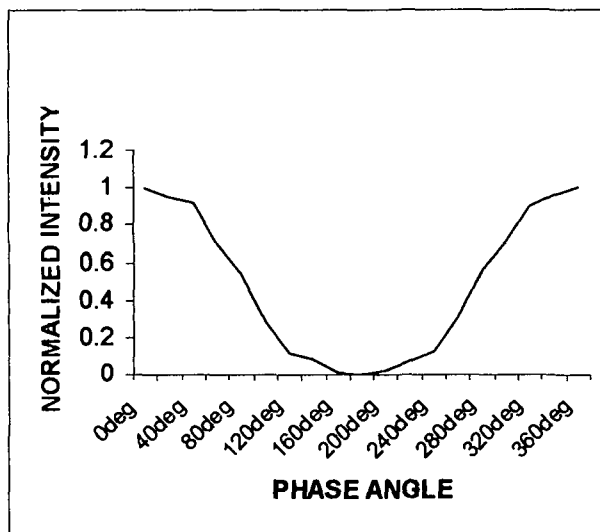
Figure 4.7.7.3. phase angle Vs normalized intensity curve
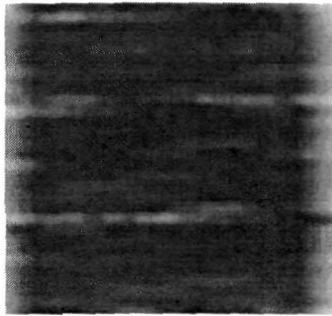
Figure4.7.7. 4. SH image of Al film surface
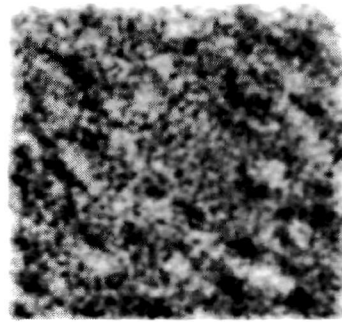
Figure4.7.7.5. SH image of Te film surface
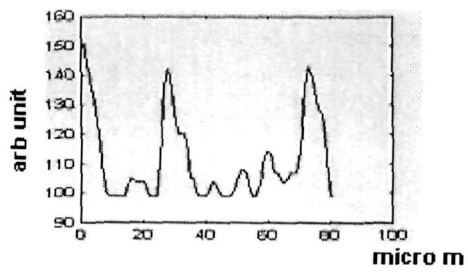
Figure 4.7.7.6 intensity profile of Figure 4.7.7.4
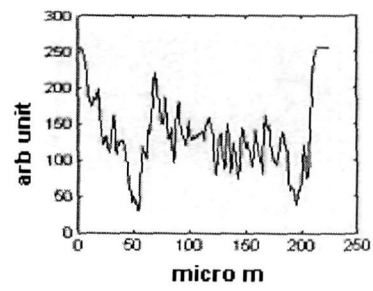
Figure. 4.7.7. 7 intensity profile of Fig 4.7.7.5

112
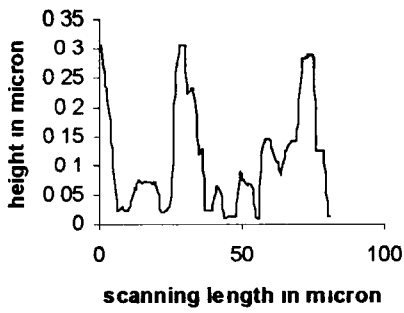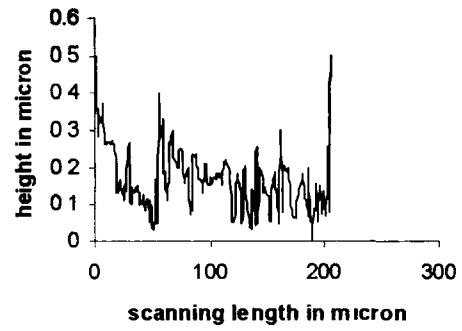
Figure4.7.7. 8   **Figure4.7.7. 9**

Figure 4.7.7.6 and 4.7.7.7: SH intensity variation with scanning length of Al and Te respectively,

Figure4.7.7. 8 and4.7.7. 9 : their topography representation
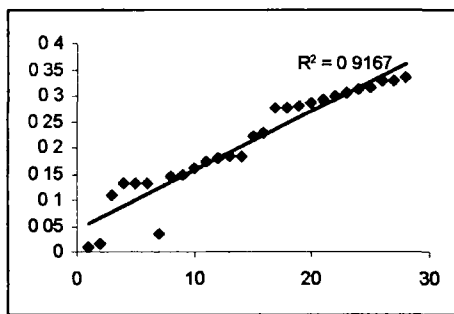
Figure 4.7.7.10 SH intensity vs Height for Al   **Figure4.7.7. 11 SH intensity Vs height for Te**
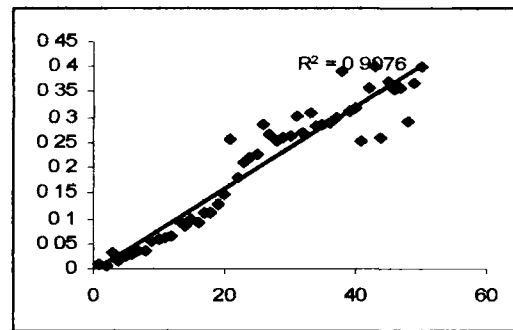
surface and also on the interaction mechanism of surface roughness and surface plasmon [75]. The enhancement of second harmonic intensity at the surface defect like bumps has been calculated by Anatoly V. Zayats et al [112]. The increase of second order nonlinear susceptibility, $\chi^{(2)}$ at the peak may be the cause of such enhancement of SH at the surface peak. The intensity of these non-linear signals falls off rapidly with the distance from the focal plane [75] which can explain the decreasing intensity at the groove of the surface.

Figure 4.7.7.10 and **Figure 4.7.7.11** show the variation of surface height for corresponding SH intensity generated at the surface of the two samples. The root mean square deviation (R^2) reveals the close proximity of the two methods for roughness measurement.

Though the SESHG and its adaptation on scanning optical microscopy is only in its initial stage, conclusion can be drawn from the above discussion that it has the probability of providing a suitable method for roughness measurement with further experimental study. But to establish it through these experiments, some problems arise as follows:

The phase shifting method is limited to shallow step heights of less than $\lambda/2$. Therefore, the sample roughness should be tested before the experiment by any other method of roughness measurement so that height variation does not exceed the $\lambda/2$ value. The roughness and flatness of the reference mirror should be far better than the sample.

It is also difficult to determine the intensity profile and topography for the same line separately. Only repeatedly performed experiments can give accurate result. However, the result will be more accurate provided SH signal and topography can be recorded simultaneously.

4.7.8.Axial resolution and Optical sectioning in SHSOM:

In the reflection geometry of a confocal scanning optical microscope, considering the object specimen as a perfect reflector, the variation of measured intensity with the axial position can be given as,

$$I(u) = \left[\frac{\sin \frac{u}{2}}{\frac{u}{2}} \right]^2$$
4.7.8.1

where $u = \dfrac{8\pi z \sin^2\left(\dfrac{\alpha}{2}\right)}{\lambda}$; u is the optical co-ordinate when the response of the reflection confocal system with defocus is considered. Here, z is the axial displacement and α is the semi angular aperture of the objective. The optical sectioning in such a confocal microscope can be achieved because light reflected from the plane axially separated from the focal plane is defocused at the detector plane and hence fails to pass through the pinhole [101].

If a conventional or type I scanning optical microscope is defocused, the image spreads out, as a result the peak intensity becomes smaller and the minima become less

prominent. So, from the point of conservation of energy, the latter no longer depends on the defocus.

But, if we consider the second harmonic scanning optical microscope, according to the three dimensional intensity equation (3.5.5), the second harmonic intensity varies with the square of the fundamental intensity and hence the effective point spread function is reduced by $\sqrt{2}$. Again the high power density with a tightly focused objective generates detectable SH only within the focal plane. So such an illumination system rejects the out-of- focus signal in SHSOM and without using an aperture in front of the detector, optical sectioning can be achieved in SHSOM. As the off- focus points do not generate SHG, it behaves like an aperture. This technique of rejecting the out –of –focus signal is named as soft aperture effect [58].

In our experiment, a thin ZnS film of thickness 20μm is taken for finding axial resolution of SHSOM. The ZnS has the tetrahedral structure. The crystal structure is cubic with 43m point group symmetry and hence it has a second order non-linearity.

A ~ 50 μm thick unpolished KDP (KH_2PO_4) crystal grown from its aqueous solution on a plane glass mirror substrate is used as a thick sample for our experiment of optical sectioning.

The SHSOM is used in its reflection mode for the measurement of axial resolution and optical sectioning. Therefore, the experimental arrangement is same as shown in the **Figure 4.7.7.1.** For axial resolution measurement, the pulsed laser light of wavelength 1.064μm is focused into the sample whose substrate is a perfectly reflected

plane mirror. The pulse width of the laser pulse is 7ns. The NA of the objective is 0.65(air). The objective (o) is moved along the z-axis in steps through a distance of f±δz by a micrometer screw fitted on its mount. The reflected SH intensity variation with the movement of the objective along z-axis is detected by the photo multiplier tube (PMT) after collecting it by the same lens (o). The peak responsivity of the photo multiplier tube is at the 550nm. The interference filter (F) of narrow band width in front of the detector prevents the exciting beam from reaching the detector.

Experimental Results:

The axial resolution curve for SHSOM is as shown in **Figure 4.7.8.1**. The FWHM of the curve predicts that the axial resolution of the microscope is within $0.6\mu m$ and $0.7\mu m$. The theoretically calculated value of lateral resolution by using equation **4.7.2.1** and fitting the data of our experiment is about 0.7061. Thus the rapid fall of axial intensity distribution curve indicates the presence of greater part of back- scattered SHG than the reflected SH light in the detected signal. Since very tightly focused beam can only give axial resolution, we repeat the experiment changing the objective of NA 0.8 and shifting the focused spot close to the sample – mirror interface which along with the thin size of the sample can optimize the reflected light in the detected signal. These modifications of our experiment improve our result and finally we have found the axial resolution to be approximately equal to 2.2.as shown in **Figure 4.7.8.2**.

The axial resolution curve gives us the idea that in case of focused excitation beam the SHG is mostly generated within a small area around the focal plane with high
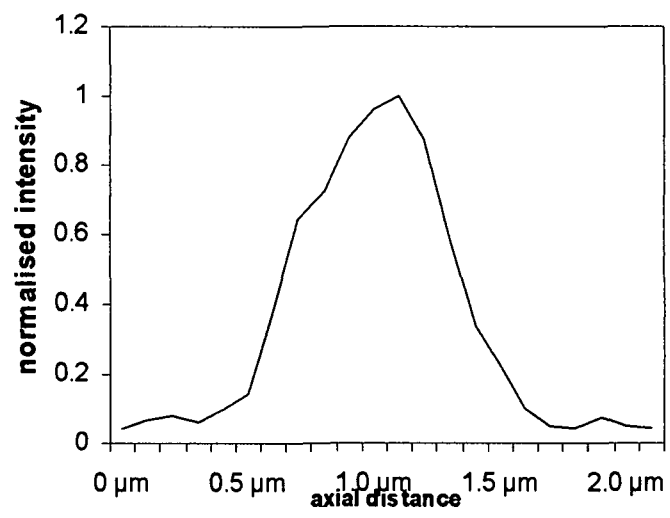
Fig 4.7.8.1 axial resolution curve for SHSOM NA of the objective is 0.65

118
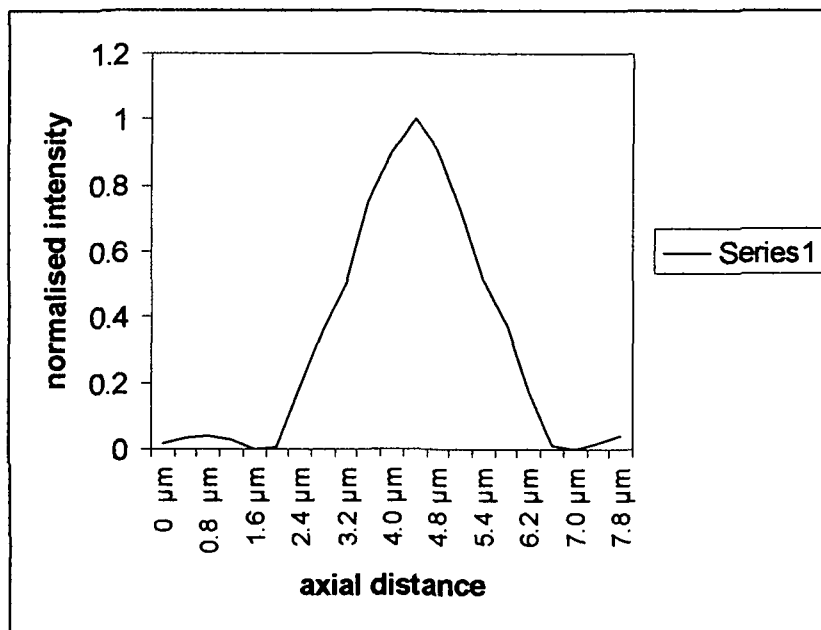
Fig 4.7.8.2 axial resolution curve for SHSOM; NA of the objective is 0.8

power density and any SHG generated outside this area can be neglected safely due its very weak intensity. Thus focusing the sample at different axial positions, and executing horizontal and vertical scanning of the sample, information of different planes in axial direction can separately be gathered resulting different images of corresponding axial planes. A 50μm thick KDP crystal is placed in the sample holder of the SHSOM working in its reflected mode. The experimental set up for optical sectioning in SH imaging is similar as illustrated in **Fig 4.7.7.1**. The objective of NA 0.8 focuses the pulsed laser radiation with a pulsed width 5ns, from the Nd- Yag laser source of wavelength1.064μm in to the sample. The x-y scanner of the SHSOM is used to scan the object in a raster form. The scanning spot is first focused on the surface of the crystal. Collecting the reflected SH signal, the SH image of the surface is obtained as shown in the **Figure 4.7.8.3(a)**. The scanning spot is shifted along the z-axis in a step of 15μm with the help of the micrometer screw and the images of different surfaces are recorded. The recorded images of these surfaces of the sample are shown in **Figure 4.7.8.3(b)**, **Figure 4.7.8.3(c)**, **Figure 4.7.8.3(d)**. Thus, we arrived at the optical sectioning by SHSOM as the images of different surfaces along z-direction inside the sample can be obtained. The computer algorithm for combining all images of different planes in the z-axis may give the 3-D images of a thick sample which is in our future plan.

Figure 4.7.8.3 (a), (b), (c),(d) the SH images of KDP crystal at four different surfaces along z-direction

121

4.8. Conclusion:

Thus, various application of SHSOM designed by us through its images proves that it has a great importance in non-linear optics (NLO).

Although better contrast and better resolution of SHI in SOM with high power laser source than those of the conventional microscope are already reported, here we have shown that these improved resolution and contrast can be obtained in the images of SHSOM with low power laser also. The resolution of the designed conventional SOM is improved by using confocal arrangement. However this has been already done by many scientists

The existence of micro crack in a sample can be detected by the second harmonic imaging mode of SOM.

The dependence of the SH intensity on second order non-linear co-efficient of the sample is utilized to calculate the latter with the help of SHI obtained from our microscope. The result coincides well with those of the known samples and hence we calculate the same for newly synthesized sample also.

Crystal defects and the impurity of the crystal can also be detected with the help of second harmonic image of our microscope.

We have illustrated here that the use of SESHG in scanning microscopy may provide a suitable method for surface probing of a sample and the location of bump and groove can be detected.

Although the optical sectioning in SHGI by femto second pulsed laser has been reported already here, we are in a position to get it in nano second range.

CHAPTER V

CONCLUSION AND FUTURE DIRECTION OF SECOND HARMONIC MICROSCOPE

5.1. Conclusion and Future Plan:

The design consideration of an improved scanning optical microscope and adaptation of second harmonic mode of imaging in it have been described in detail. We have observed second harmonic images of different types of samples. The samples include inorganic crystals like KDP, ADP etc., organic crystal (urea), semi conductors like ZnS, Te etc. Improved resolution and contrast of these second harmonic images are observed in comparison to those observed through conventional microscopes. Various applications of second harmonic scanning optical microscope like measurement of effective second order non-linear co-efficient, detection of crystal defects and impurity, detection of surface defects like bump or groove using surface enhanced second harmonic generation and optical sectioning are discussed on the basis, of some experiments. As the SHG microscopy is not yet a mature field and its work is in progress only, its applications are still being discovered. The second-order co-efficients of different biological materials vary over an enormous range and hence second harmonic images show very high contrast in biological samples which help in studying different tissue structures [50],[53],[54],[55] and also in disease diagnosis [59].

In our future view point, we expect the second harmonic imaging of biological specimen making suitable arrangement necessitated by it. The high input laser power

required for SHG is not suitable for the study of fragile and sensitive specimen such as biological tissues [75]. Although, the high peak power of short pulses can generate maximum second harmonic for a given average input power, photo damage of the sample is induced from such extremely strong optical flux. To achieve efficient SHG from biological samples, femtosecond laser pulses through high numerical aperture of the microscope is routinely used. But the local interaction between biological samples with light under such strong optical field causes permanent damage of the sample very easily. Konig et al. have demonstrated that the loss of cell viability occurred at an average power of ~ 7 mW for 150 fs pulses (with a 80 MHz repetition rate), corresponding to a peak power of 0.56 KW, or a pulse energy of ~0.1 nJ [113]. In the same study they also verified the non-linear nature of the optical damage in the femtosecond pulse regime.

Though the minimum pulse width of our Nd-Yag source is only 2.5ns, its very high peak power of the order of tens of mega Watt induces photo damage very easily. For adequate SHG we have to use the source with minimum pulse width which supplies the maximum peak power. The low repetition rate (frequency) of only 10 Hz of the source is another difficulty. The desired high average intensity of SHG and unwanted non-linear photo damage can be best balanced by increasing the repetition rate of laser. With identical peak intensity and pulse energy in each pulse, the mean power of emitted SHG will linearly increase with the increase of repetition rate while no non-linear photo damage will take place if the peak intensity and pulse energy is kept well below the photo damage threshold [73]. Addition of such an arrangement in our experimental set-up may help us to view biological samples under SHSOM.

Three dimensional reconstruction of these images is also expected in our future plan by improving our optical sectioning property of the microscope, discussed in the section **4.14.** The three dimensional reconstruction can be possible by the use of Voxel View program on a Silicon Graphics Indigo 2 workstation [58]. The improvement of resolution of such images is also expected by making confocal configuration to the detected path in SHG.

REFERENCES

1. "Historical Introduction" by W.E.Watson-Baker in *"The microscope: its history and applications"*(Whitefriars press Ltd.)

2. *"Development of the Microscope"*; Copyright © 1994-2002 Encyclopaedia Britannica, Inc.

3. J.Z. Young and F. Roberts, *Nature* **167**, 231 (1951)

4. R. Barer , *Nature* **169**; 366 (1952)

5. L.L.Hundley, Ann. N.Y. *Acad. Sci.* **97**, 514 (1962)

6. L. J. Laub, *J. Opt. Soc. Am.* **62**, 737 (1972)

7. *S. Polze, *Monatsber Deutschen Akad.* Wiss. Berline, **7**, 631 (1965)

8. E. M. Deely, *J. Sci. Instr.* **32**, 263 (1955)

9. H.C. Box and H. Freund, *Rev. Sci Instrum.* **30**, 28 (1959)

10. J.A. Dobrowolski, W. Godfrey, P.N. Slater and W. Weinstein, *J. Opt. Soc. Am*, **47**, 186 (1957)

11. P. N. Slater, *J. Opt. Soc. Am*, **49**, 562 (1959)

12. W. T. Welford, *Optics in metrology* (Ed. by P. Mollet, 85, Pergamon press, Oxford) (1960)

13. P. Montogomery, F. Roberts and W. Bonner, *Nature* **177**, 1172 (1956)

14. V. K. Zworykin and F. L. Hatke, *Science* **126**, 805 (1957)

15. G.R. Price and S. Schwarz, *Physical techniques in biological research* **3**, 91 (1956)

16. M. Minsky, U.S. patent 3013467, *Microscopy apparatus Dec.* **19**, (1961) (filed Nov. 7, 1957)

17. M.D. Egger and Petran, *Science* **157**, 305 (1967)

18. T.O. Caspersson and G.M. Lomakka, *Ann. N. Y. Acad. Sci.* ;**97**; 449 (1962)

19. P. Davidovitz and M. D. Egger, *Nature* **223**, 831 (1969)

20. P. Davidovitz and M. D. Egger, *Appl. Optics*, **10**, 1615 (1971)

21. *H. Beyer, *Jenaer Johrbuch* 185 (1966)

22. A. Korpel and R. L. Whitman, *Appl. Optics*, **8**, 1577 (1969)

23. E. Ash and G. Nicholls, *Nature*, **237**, 510 (1972)

24. *A. Handi, J. M. Bassia, X. Gerbaux and R. Thomas, *Appl. Optics*, **15**, 2150 (1976)

25. C. J. R. Sheppard and R. Kompfner; *Applied Optics*; **17**, 2879 (1978).

26. A. Choudhury and C.J. R. Sheppard; *Optica Acta*; **24**, 1051 (1977).

27. A. Choudhury; Doctoral thesis; Oxford University; (1977).

28. G. J. Brakenhoff, J. S. Binnerts, Woldringh; *"Scanned Image Microscopy"*(E.A. Ash, ed.) 183 Academic press, London and New York. (1980)

29. K. Carlsson.,P.E. Danielsson, R. Lenz., A. Liljeborg., L. Majlof and N. Aslund.; *Optics Lett.* **10**, 53ʹ(1985).

30. T. Wilson and D. K. Hamilton; *J. Microscopy* **128**, 139 (1982)

31. C. J. R. Sheppard and D. K. Hamilton; *Appl. Optics* **22**, 886 (1983)

32. I.J. Cox, C.J.R. Sheppard; *Appl. Optics* **22**, 1474 (1983b)

33. *H. Caulfield, D.L. Kryger; *Proc. Soc. Photo-opt. Instrum. Eng* **153**, 23; (1978).

34. D. K. Hamilton and T. Wilson; *Appl Phys* **53**, 5320 (1982a)

35. J.P. Fillard; *Near Field Optics and Nanoscopy;* World Scientific Publishing Co. Pte. Ltd. Singapore. New Jersey. London. Hong Kong (1998).

36. E. H.Synge; *Phil. Mag* **6**; 356 (1928)

37. Thierry Pagnot, Dominique Barchiesi, Daniel Van Labeke and Christian Pieralli; *Optics Letter* **81**, No 7, 2929 (1997)

38. Ulrich D. Keil, Jacob R. Jensen and Jorn M. Hvam; *J of Appl. Phys* **81**. No.7 ,2929 (1997)

39. G. Binnig., C.F.Quate, Ch Gerber; *Phys Rev. Lett* **56** 930 (1986)

40. E.A.Ash. "*Scanned Image Microscopy*"- Acad. Press London (1980)

41. G. Dolino, J.P. Bachheimer, M. Vallade; *Applied Physics Letters* **22**, 623 (1973)

42. G. Dolino, *Applied Physics Letters* **22**, 123 (1973).

43. R. Hellwarth, P.Christiansen; *Optics Communications* **12**, 318 (1974).

44. J. Gannaway, C.J.R. Sheppard, *Optical and Quantum Electronics* **10**, 435 (1978).

45. T. Jentsch, H.J. Jupner, S.H. Ashworth, T. Elsaesser; *Optics Communications* **138**, 341 (1996).

46. D.J. Bottomley, A. Mito, S. Niki, A. Yamada; *Optics Letters* **21**, 254 (1996).

47. J.Vydra, M. Eich; *Applied Physics Letters* **72**, 275 (1998)

48. S. Janz., K. Pedersen, van Driel, H.M., *Physical Review* B **44**, 3943 (1991).

49. S.D. Moustaizis, N.A. Papadogiannis, C. Fotakis, G. Farkas, C. Toth; *Applied Physics Letters* **67**, 3239 (1995).

50. Derr VE, Klein E, Fine S; *Fedaration Proc* **24** (suppl 14); S 99 (1965).

51. Zaret M.M; *Federation Proc* **24** (suppl 14); S 62 (1965)

52. Fine S and Hansen WP; *Apl. Opt* **10**, 2350 (1971)

53. Y. Guo, P.P. Ho, A. Tirksliunas, F. Liu, R.R. Alfano; *Applied Optics* **35**, 6810 (1996).

54. Y. Guo, Q.Z. Wang, N. Zhadin, F. Liu, S. Demos, D. Calistru, A. Tirksliunas, A. Katz, , Y. Budansky, P. Pho, R.R. Alfano; *Appl Opt* **36**, 968 (1997a)

55. Y. Guo, P.P. Ho, H. Savage, D. Harris, P.Sacks, , S. Schantz, F. Liu, N. Zhadin, , R.R. Alfano; *Optics Letters* **22** , 1323 (1997b).

56. I. Freund, M. Deutsch, A. Sprecher; *Biophysical Journal* **50**, 693 (1986).

57. J. Mertz, L. Moreaux, T. Pons, Proc. SPIE 4620, 182, (2002)

58. R. Gauderon, P.B. Lukins, C.J.R. Sheppard. *Optics Letter* **23**, No.**15**; 1209 (1998)

59. Xiaoyvan Deng, Elizabeth D. Williams, Eric W. Thompson, X. Gan, Min Gu; *Scanning;* **24**, 175 (2002).

60. W.T. Welford; "Theory and Principles of Optical Scanning Microscopy"; Scanned Image Microscopy, edited by Eric A. Ash; Academic Press, London, 165 (1988)

61. C.J.R.Sheppard; "Imaging Modes of Scanning Optical Microscopy"; Scanning Image Microscopy, edited by Eric A. Ash; Academic Press, London, 201 (1988)

62. T.Wilson, J.N. Gannaway and C.J.R.Sheppard; "Scanning Optical Microscopy of Semiconductor Devices"; Scanned Image Microscopy, edited by Eric A. Ash; Academic Press, London, 227 (1988).

63. C. J. R. Sheppard, T. Wilson; *Applied Optics*; **18**, No.7,1058 (1979).

64. C.J.R. Sheppard, X.Q. Mao, *Journal of Modern Optics*, **35**, No. 7, 1169 (1988).

65. R. Bachelot, P. Gleyzes, A.C. Boccara; *Applied Optics*; **36**, No. 10, 2160 (1997).

66. Dominique Barchiesi, Oliver Bergossi, Michel Spajer, Christian Pieralli; *Applied Optics*, **36**, No. 10, 2171 (1997).

67. Ragnar Erlandsson and Peter Apell; *Current Science*: **78**, No. 12, 1445 (2000).

68. June- hyoung Park, Myong R. Kim, Wonho Jhe; *Optics Letters*, **25**, No.9, 628 (2000).

69. M. Martinez Corral, C.Ibanez- Lopez,G. Saavedra, M.T. Caballero; *Optics Express*, **11** No. 19, 1740 (2003).

70. *Oarles J. Koester; *Applied Optics*; **19** No. 11, 1749

71. Bernard Grob; "*Basic Television and Video Systems*"; Fifth Edition; McGraw-Hill Book Company; International Student Edition; 25 (1984).

72. D.N. Basudeva; "*Fundumentals of Magnetism and Electricity*", Eleventh Revised Edition, S. Chand and company Ltd. 338 (1982).

73. Shi-Wei Chu, Tzu-Ming Liu and Chi-Kuang Sun, Cheng-Yung Lin and Huai-Jen Tsai **11** No. 8, OPTICS EXPRESS, 933 (2003)

74. D.N. Basudeva; "*A Text Book of Light*", Fifth Edition; Atma Ram & Sons Publishers, Delhi; 419 (1962).

75. R. Gauderon, P.B. Lukins, C.J.R. Sheppard; *Micron* **32**, 691 (2001).

76. *L. Moreaux, O. Sandre, S. Charpak, M. Blanchard- Desce, and J. Mertz; *Biophys. J.*, **80**, 1568 (2001).

77. *W. T. Welford; *Journal of Microscopy* **96**, 105 (1972).

78. *G E Solid State Data Book on Optoelectronics*; GE/ RCA/ Intersil Semiconductors, 19, 186 (1987).

79. *Laboratory Manual of Photo –Multiplier-Tube*; Scientific Equipment & Services; Roorkee ; India, 2, (2004).

80. B.L.Theraja; "*Basic Electronics Solid State*"; Fourth Edition(reprinted), S. Chand & Company Ltd, 783 (1991).

81. Ramakanta A. Gayakward; *"Op- Amps and Linear Integrated Circuits"*; Third Edition; Prentice Hall of India, Private Ltd.

82. A. K. Sawhney; "A Course in Electrical and Electronics Measurements and Instrumentation"; Fifth Edition, Dhanapat Rai & Sons, New Delhi, 844 (1988).

83. Roy Edwards; *"Discovering Electronics An Active- Learning Approach"*, D.P Publications Ltd. Aldine Place, London W 128 AW, 172, 273 (1994).

84. Probir Goyal; *Electronics For You*, Oct, 96 EFY Enterprises Pvt Ltd , New Delhi; 87 (1996).

85. Henry W. Ott; *"Noise Reduction Techniques in Electronics Systems"*; Second Edition; A. Wiley – interscience Publication(John Wiley & Sons); 1989.

86. M.E.Barnet; *Journal of Microscopy* ,**102**,1, (1974)

87. J.W. Goodman, *"Introduction to Fourier Optics"*; McGraw Hill (1968)

88. C.J.R. Sheppard; *IEEE, Journal of quant Elec. QE-* **13**, 49D, (1977a)

89. C.J.R. Sheppard and T.Wilson; *Applied Optics*, **18**, 3764, (1979a)

90. H.H. Hopkins and P.M. Barham; *Proc. Phys. Soc*, **63**, 72, (1950)

91. Rayleigh, Lord, *Phil. Mag*, (5) **42**, 167, (1896)

92. T.S. McKechnie; *Optica Acta*, **19** , 729, (1972)

93. D.A. Kleinman, *Physics Review*, **128**, 1761 (1962).

94. Walter Koechner; *"Springer Series in Optical Sciences. Solid- state Laser Engineering"*

95. Christopher C. Davis; *Laser and Electro-optics Fundamentals and Engineering* the Press Syndicate of the University of Cambridge, (1996).

96. A. Yariv., *Quantum Electronics*, Wiley, New York, (1967)

97. Boyd and Gordon, Bell system technical journal, $\underline{40}$, 489, (1966)

98. Bernd Jahne; "*Practical Handbook on Image Processing for Scientific Applications*", CRC Press LLC; USA (1997)

99. J.P. Fillard; *Near Field Optics and Nanoscopy;* World Scientific Publishing Co. Pte. Ltd. Singapore. New Jersey. London. Hong Kong 75 (1998).

100. R.W. Munn and C.N. Ironside; "*Principles and Applications of Non-linear Optical Materials*"; Blackie Academic & Professional; (1993).

101. C. J. R Sheppard.; "*Scanning Optical Microscopy, in Advances in Optical and Electron Microscopy*", $\underline{10}$, R Barer and VE Cosslett eds. Academic Press, London, 1, (1987).

102. Brown F, Parks R. E, Sleeper A.M.; Phys. Rev. Lett. $\underline{2}$, 1092(1965).

103. A. Sarmah Goswami, G.A. Ahmed, A. Choudhury; Journal of Optics, $\underline{33}$. No. 1, 29 (2004)

104. Mertz Jerome, Laboratorie de Neurophysiologie et Nouvelles Microscopies INSERM, France., " Second harmonic generation microscopy", web page: www.physio.espci.fr; date 13 May, (2003)

105. Sharada G Prabhu and P. Mohan Rao; Journal of Optics; $\underline{29}$ No.4; 193 (2000).

106. M. Narayan Bhat and S.M. Dharmaprakash; Journal of Optics, **31**, No. 4; 159 (2002).

107. Leonid V. Zhigilei; *"Introduction to Material Science, Chapter 4, Imperfections in solids"*, Department of Materials Science and Engineering University of Tennessee.

108. Robert M. Corn and Daniel A. Higgins, Chem. Rev. **94**, 107 (1994).

109. T.F. Heinz.; *"Nonlinear Surface Electromagnetic Phenomena"*, edited by Ponath, H.E. Stegeman, G. I.; North Holland, Amsterdam (1991)

110. V. Mizrahi., J. E. Sipe; J. Opt. Soc. Am. B 660 (1988)

111. C.J.R. Sheppard, R. Kompfer, J. Gannaway, D. Walsh, IEEE J. Quantum Electron, 13E,100D, (1977)

112. Anatoly V. Zayats, Thomas Kalkbrenner, Vahid Sandoghdar, Jurgen Mlynek, Physical Rev B. **61**, No.7, 4545 (2000).

113. Koing, T.W. Becker, P. Fischer, I. Riemann and K.J.Halbhubar ; Opt Lett, **24** 113 (1999).

114. T. Wilson and C.J.R. Sheppard *"Scanning Optical Microscopy"* in Analysis of Microelectronic Materials and Devices., edited by M. Grasserbauer and H.W. Werner, John Wiley and Sons Ltd. (1991).

*' indicates cross reference.

PUBLICATIONS:

1. A.S. Goswami, G. A. Ahmed and A. Choudhury, Super Resolution and Better Contrast in Second Harmonic Scanning Optical Microscope with Low Power Laser Beam, *Journal of Optics* , Vol. 33, No. 1 (2004), 29- 35

2. A.S. Goswami, G. A. Ahmed and A. Choudhury, Measurement of Second Order Non-linear susceptibility of matter with the help of SHSOM (to be published in Indian Journal of Physics)

Presentations:

1. A.S. Goswami, G. A. Ahmed and A. Choudhury, Second Harmonic Scanning Optical Microscope as a Tool of Roughness Measurement, National Conference on Materials and their Applications (NCMA-2004), March 11- 13, 2004), Department of Physics, Kurukshetra University, Kurukshetra.

2. A.S. Goswami, G. A. Ahmed and A. Choudhury, Measurement of Second Order Non-linear susceptibility of matter with the help of SHSOM, Condensed Matter

Days-2004 (25-27 August, 2004), Department of Physics, North- Eastern Hill University, Shillong.

3. A.S. Goswami, G. A. Ahmed and A. Choudhury, Design of a Scanning Optical Microscope in its Second Harmonic Mode of Imaging and the Measurement of Effective Second Order non-linear Co-efficient of Matter, talk delivered as a TPSC (Theoretical Physics Seminar Circuit) speaker, 7th March, 2005, Institute of Physics, Bhubaneswar

4. Axial Resolution in the Second Harmonic Scanning Optical Microscope and Optical Sectioning, seminar lecture in UGC sponsored Refresher Course, (8-28 Dec, 2003), Gauhati University, Guwahati.